ASME Applied Mechanics Reviews
Online journal at:
https://asmedigitalcollection.asme.org/appliedmechanicsreviews

Statistical Scaling in Localization-Induced Failures

Jia-Liang Le
Department of Civil, Environmental, and Geo-Engineering,
University of Minnesota,
Minneapolis, MN 55455

The investigation of statistical scaling in localization-induced failures dates back to da Vinci's speculation on the length effect on rope strength in 1500 s. The early mathematical description of statistical scaling emerged with the birth of the extreme value statistics. The most commonly known mathematical model for statistical scaling is the Weibull size effect, which is a direct consequence of the infinite weakest-link model. However, abundant experimental observations on various localization-induced failures have shown that the Weibull size effect is inadequate. Over the last two decades, two mathematical models were developed to describe the statistical size effect in localization-induced failures. One is the finite weakest-link model, in which the random structural resistance is expressed as the minimum of a set of independent discrete random variables. The other is the level excursion model, a continuum description of the finite weakest-link model, in which the structural failure probability is calculated as the probability of the upcrossing of a random field over a barrier. This paper reviews the mathematical formulation of these two models and their applications to various engineering problems including the strength distributions of quasi-brittle structures, failure statistics of micro-electromechanical systems (MEMS) devices, breakdown statistics of high– k *gate dielectrics, and probability distribution of buckling pressure of spherical shells containing random geometric imperfections. In addition, the implications of statistical scaling for the stochastic finite element simulations and the reliability-based structural design are discussed. In particular, the recent development of the size-dependent safety factors is reviewed.* [DOI: 10.1115/1.4065668]

1 Introduction

The phenomenon of localization is a ubiquitous characteristic of damage and failure of many engineering structures and devices. Some common examples include damage in concrete specimens under tension [1,2], formation of a shear band or compression band in rock specimens under uniaxial compression [3–5], diagonal shear failure of reinforced concrete beams [6–8], localized buckling of spherical shells [9–12], trap-assisted tunneling in gate dielectrics under voltage [13–15], etc. Understanding the physics of these localization phenomena, which is of critical importance for the analysis and design of different engineering structures and processes, has attracted a vast amount of research efforts over the past half-century. Significant advances have been made in all fronts of mathematical modeling, numerical simulations, and experimental characterization of various localization behaviors in failure of materials and structures.

In structural mechanics, localization as a form of instability can arise from inelastic material behavior as well as from geometric nonlinearity. The mathematical analysis of localization instability due to nonlinear material behavior dates back to Hill's work on localized necking in plastic sheets [16]. Rudnicki and Rice developed a rigorous mathematical approach, (i.e., the acoustic tensor), for determining the onset of localization instability in the case of hardening plasticity [17]. The concept of acoustic tensor was later applied to quasi-brittle materials, which exhibit a strain-softening constitutive behavior [18,19]. During the same period of Rudnicki and Rice's work, Bažant pioneered the analysis of the localization instability for brittle heterogenous (a.k.a. quasi-brittle) materials [1]. He pointed out that localization instability could lead to spurious mesh sensitivity in continuum finite element (FE) simulations. This discovery led to the development of a class of computational methods, commonly referred to as the localization limiters, for suppressing the mesh sensitivity. Some notable methods include the crack band models [2,20–23], nonlocal integral models [24–26], and explicit and implicit gradient models [27–31]. The other important consequence of localization instability in quasi-brittle materials is the dependence of the failure behavior on the structure size. This size effect was studied extensively for various quasi-brittle structures exhibiting different failure modes [32–35].

In addition to nonlinear material behavior, geometric nonlinearity could also lead to localization instability. A commonly seen example is the elastic buckling of cylindrical and spherical shells. Even for a linear material model, the bifurcation analysis of post-buckling behavior, which usually involves a system of coupled PDEs, is very complicated [11,12,36]. The analysis of shell buckling is further complicated by the fact that many shells contain geometric imperfections leading to a significant reduction in the critical buckling load. In recent studies, high-fidelity computational models were used for both deterministic and stochastic analyses of localized buckling behavior of shells with geometric imperfections (or defects) [36–39]. These analyses revealed some important features including the effect of imperfection size on the buckling load, the influence of defect interaction on the buckling behavior, and the geometric characteristics of the localized buckling zone.

One common macroscopic feature of the aforementioned localization-induced failures is that the load capacity of the structure decreases once the localization occurs. Meanwhile, there are many possible locations, where localization could happen. The actual

Manuscript received May 1, 2024; final manuscript received June 2, 2024; published online June 26, 2024. Assoc. Editor: Yonggang Huang.

location of localization zone is intrinsically random. This phenomenon indicates that the statistics of the failure load are intimately related to the stochastic nature of the localization behavior. In fact the effect of localization on failure statistics has been studied much longer ago, dating back to da Vinci's famous speculation on the effect of length of a rope on its load capacity [40]. About a century later, Marriott provided a qualitative explanation for this speculation, in which he stated that such a length effect is plausible if one considers there is some weak spot in the rope due to material inhomogeneity [41]. This was the first discussion of what is now known as the statistical size effect. The quantitative description of statistical size effect came much later. The mathematical foundation of this size effect was laid down by Fisher and Tippett in their ground-breaking work on the extreme value statistics [42]. Weibull independently proposed an extreme value distribution, now referred to as the Weibull distribution, through extensive experimental investigations into the strength distributions of porcelain, cotton, wood, and cement mortar [43]. The Weibull distribution naturally yields a size effect model, which describes the dependence of mean structural strength on the structure size [43,44].

Over the past four decades, there has been abundant experimental evidence showing that the Weibull distribution does not provide optimum fits of strength distributions of many quasi-brittle materials including concrete, engineering and dental ceramics, fiber composites, cold asphalt mixtures, and polycrystalline silicon (poly-Si) at the microscale [34]. This is because the Weibull distribution is anchored by the extreme value statistics, which implies that the localization zone must be negligibly small as compared to the size of test specimens. This condition is usually not met for laboratory test specimens. To address this issue, a finite weakest-link model was proposed for probability distributions of strength and lifetime of quasi-brittle materials [45–48]. The Weibull distribution was shown to be the limiting case of the finite weakest-link model. The model matches well the experimentally measured strength and lifetime distributions of quasi-brittle materials. The essential consequence of the model is that it predicts an intricate size effect on the probability distribution function of the structural strength. The Weibull size effect represents the limiting form of the mean size effect curve at the large-size asymptote.

The finite weakest-link model was derived by considering a set of discrete and statistically independent random variables, which represent the random resistances corresponding to the onset of localization at different possible locations. In recent studies [49–51], a level excursion model was developed for the statistics of extreme value of a continuous random field, which exhibits spatial correlation. Because the model directly deals with the continuous random field, the model is able to capture the size effect behavior over the entire size range including the small-size asymptote, which cannot be predicted by the finite weakest-link model.

Though the recent developments of the finite weakest-link model and level excursion analysis are motivated by the need for understanding the strength distribution of quasi-brittle structures, it was found that these mathematical models are applicable to a wide range of localization-induced failures of engineering structures. This review paper will discuss the general mathematical framework of the finite weakest-link model and level excursion analysis, the consequent statistical scaling behavior, and their engineering applications.

2 Mathematical Framework

Let ψ_c denote the structural resistance defined in a broad sense. For instance, in structural mechanics, ψ_c usually refers to the peak load capacity of the structure. In the case of electrical breakdown, ψ_c could denote the maximum voltage or current that the device can sustain. Since the failure happens at the onset of localization at one location, the formation of each potential localization zone would correspond to one resistance value. The overall resistance ψ_c is equal to the minimum of the resistance values corresponding to the onset of localization at all possible locations, i.e.,

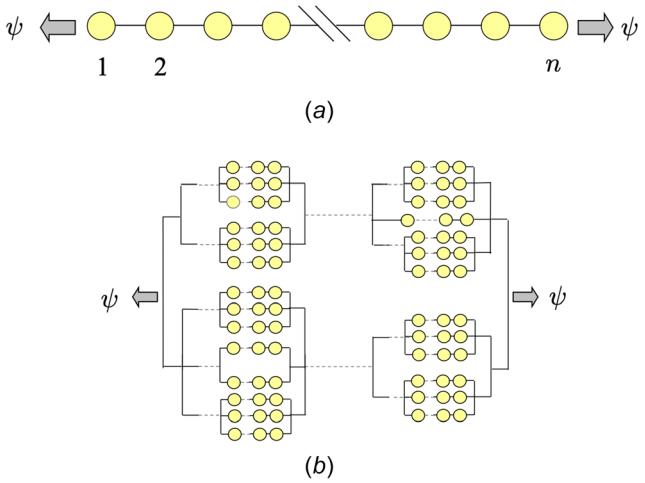

Fig. 1 Concept of finite weakest-link model: (*a*) chain model for macroscopic structure, and (*b*) hierarchical model for the resistance corresponding to the formation of one particular localization zone

$$\psi_c = \min(\psi_1, \ldots, \psi_n) \tag{1}$$

where ψ_i = resistance value for the formation of a localization zone at location i, and n = number of possible locations of localization onset in the structure. Due to the random material heterogeneities (e.g., microstructures), ψ_i are intrinsic random variables. The randomness of ψ_c is related to the randomness of ψ_i as well as to the number of possible locations of the localization zone. The goal is to determine the cumulative distribution function (cdf) of ψ_c.

2.1 Finite Weakest-Link Model. In the simplest setting, we can consider that ψ_i's are independent and identically distributed random variables. Equation (1) indicates that, for the purpose of calculating the cdf of ψ_c, the structure can be regarded as a chain of elements, each of which represents one potential localization zone (Fig. 1(*a*)). Based on the joint probability theorem, the cdf of ψ_c can then be written by

$$1 - P_f(\psi) = [1 - P_1(\psi)]^n \tag{2}$$

where $P_f(\psi) = \Pr(\psi_c \le \psi)$ = cdf of the resistance of the entire structure, and $P_1(\psi) = \Pr(\psi_i \le \psi)$ = cdf of the resistance corresponding to the formation of one particular localization zone. Equation (2) represents the fact that the structure would not fail if and only if not a single localization zone has formed.

In the context of extreme value statistics, it is of interest to consider the limiting case of $n \to \infty$. When n is large, $P_f(\psi)$ is determined by the far left tail of $P_1(\psi)$. By taking the logarithm of both sides of Eq. (2) and using the fact $\ln(1-x) \approx -x$ for $x \to 0$, we can rewrite Eq. (2) as

$$P_f(\psi) = 1 - \exp[-nP_1(\psi)] \tag{3}$$

Meanwhile, the distribution function $P_f(\psi)$ must satisfy the stability postulate [42]. In this postulate, we divide the structure domain into p subdomains, where each domain contains q number of potential localization zones. Since the total number of potential localization zones, n, approaches infinity and p is finite, we must have $q \to \infty$. Using the joint probability theorem, we can relate $P_f(\psi)$ to the failure probability of one subdomain $P_g(\psi)$, i.e.,

$$1 - P_f(\psi) = [1 - P_g(\psi)]^p \tag{4}$$

Since both the entire structure and the subdomain contain an infinite number of potential localization zones, the probability distribution

functions $P_f(\psi)$ and $P_g(\psi)$ must be related to each other by a linear transformation of the random variable, i.e., $P_g(\psi) = P_f(a_p\psi + b_p)$, where a_p, b_p = constants dependent on the value of p. Therefore, Eq. (4) becomes

$$1 - P_f(\psi) = [1 - P_f(a_p\psi + b_p)]^p \tag{5}$$

Equation (5) is a functional equation, referred to as the stability postulate. It states that, as $n \to \infty$, $P_f(\psi)$ converges to a particular functional form.

Based on Eq. (3), the essential problem is to find $P_1(\psi)$ that would satisfy the stability postulate (Eq. (5)). The left-tail of distribution function $P_1(\psi)$ is commonly known as the domain of attraction [42,52–54]. Gnedenko gave the conditions for function $P_1(\psi)$ to converge to an extreme value distribution [55]. It has been shown that three types of tail distributions, namely, the exponential tail, the polynomial tail, and the power-law tail, can fulfill this requirement [42,52,53,56]. These distribution tails lead to the Gumbel, Fréchet, and Weibull distributions, respectively. Though these three distributions are not exhaustive, they are sufficient for most (if not all) practical engineering problems.

Both the exponential and polynomial tail distributions extend to negative values of the random variable, which cannot be applied to structural resistance. Therefore, the only choice for $P_f(\psi)$ is the Weibull distribution, i.e.,

$$P_f(\psi) = 1 - \exp\left\{-n\frac{\langle\psi - \psi_0\rangle^m}{s_0^m}\right\} \tag{6}$$

where $\langle x\rangle$ = Macaulay bracket, m = Weibull modulus, s_0 = Weibull scale parameter, and ψ_0 = resistance threshold. Without resorting to the stability postulate, Weibull proposed the power-law tail distribution for $P_1(\psi)$ and consequently Eq. (6) for the strength distribution of engineering materials including porcelain, cotton, wood, and cement mortar, as well as for the probability distribution of spark voltage between spherical electrodes, through his extensive experimental campaign [43]. An important result of Weibull's work is the size effect on the mean structural resistance, i.e.,

$$\bar{\psi}_c = \int_0^1 \psi \mathrm{d}P_f(\psi) \tag{7}$$

$$= \int_0^\infty [1 - P_f(\psi)]\mathrm{d}\psi \tag{8}$$

Equation (8) uses the fact that ψ is non-negative. By substituting Eq. (6) into Eq. (8), we obtain

$$\bar{\psi}_c = \psi_0 + s_0\Gamma\left(1 + \frac{1}{m}\right)n^{-1/m} \tag{9}$$

where $\Gamma(x)$ = gamma function. In most cases, we have $\psi_0 = 0$, and Eq. (9) leads to a power-law scaling relation: $\bar{\psi}_c \propto n^{-1/m}$. The power-law form stems from the fact that here we consider the size of localization zone to be negligibly small as compared to the overall structure size (i.e., n is very large). In the absence of a characteristic length (i.e., size of localization zone), the scaling relation must follow a power law [35,57,58]. This power-law size effect on the mean resistance is known as the Weibull statistical size effect. Its physical significance is that this size effect on the mean behavior is governed purely by statistics, which cannot be captured by any deterministic model.

The foregoing analysis focuses on the case of $n \to \infty$, which corresponds to the framework of the extreme value statistics. For many structures, the size of localization zone is not negligibly small as compared to the structure size. In a general setting, we must treat n in Eq. (1) to be finite. This leads to the finite weakest-link model, which has recently been developed for the strength statistics of quasi-brittle structures. Nevertheless, the modeling framework is widely applicable to other localization phenomena. When n is finite, we need to know the entire distribution function $P_1(\psi)$. As discussed, $P_1(\psi)$ should have a power-law tail. Clearly, the theory of extreme value statistics does not provide any information about the core portion of $P_1(\psi)$. In recent studies [34,45–48], a hierarchical statistical model was developed to determine the functional form of $P_1(\psi)$ (Fig. 1(*b*)). The model consists of a hierarchy of bundles and chains representing the averaging and localization effects at different material scales. The outcome of the model is that the core of $P_1(\psi)$ can be approximated by a Gaussian distribution. Therefore, it was proposed to model $P_1(\psi)$ by a Gaussian-Weibull distribution, i.e.,

$$P_1(\psi) = \begin{cases} (\psi/s_0)^m & (\psi \le \psi_g) \quad (10a) \\ P_g + \dfrac{r_f}{\delta_0\sqrt{2\pi}}\displaystyle\int_{\psi_g}^{\psi} e^{-(x-\mu_0)^2/2\delta_0^2}\mathrm{d}x & (\psi > \psi_g) \quad (10b) \end{cases}$$

where μ_0 and δ_0 are the mean and standard deviation of the Gaussian core if considered extended to $-\infty$; r_f is a scaling parameter required to normalize the grafted cdf such that $P_1(\infty) = 1$, ψ_g = grafting stress, and $P_g = (\psi_g/s_0)^m$ = grafting probability. We further require the continuity of the probability density function (pdf) at the grafting point, i.e., $[\mathrm{d}P_1/\mathrm{d}\psi]_{\psi_g^+} = [\mathrm{d}P_1/\mathrm{d}\psi]_{\psi_g^-}$.

By substituting Eqs. (10*a*) and (10*b*) into Eq. (1), we calculate the probability distributions of structural resistance for different values of n, as shown in Fig. 2(*a*). Note that, in many localization-induced failures (one exception is shell buckling, which will be discussed later), the size of localization zone represents a characteristic length scale, which is independent of the structure size. Therefore, we can interpret n as a dimensionless descriptor of structure size. It is seen that, as n increases, the probability distribution of ψ_c transitions from a predominantly Gaussian distribution with a power-law tail to a Weibull distribution. Clearly, the classical extreme value statistics is the limiting case of the finite weakest-link model. Since the size of localization zone is a fixed length scale, the size effect on the mean structural resistance would necessarily deviate from the power-law, as shown in Fig. 2(*b*). An approximate equation was proposed to describe the mean size effect [34,45,46]

$$\bar{\psi}_c = \psi_0\left[\frac{n_1}{n} + \left(\frac{n_2}{n}\right)^{r/m}\right]^{1/r} \tag{11}$$

where ψ_0, n_1, n_2, r =constants. By matching the small and large size asymptotic behaviors, these constants can directly be related to the statistical parameters of the distribution function $P_1(\psi)$ [59]. When $n \to \infty$, Eq. (11) reduces to $\bar{\psi}_c \propto n^{-1/m}$, i.e., the Weibull size effect.

Moreover, the finite weakest-link also predicts the size effect on the standard deviation of ψ_c. Similar to the mean resistance, a closed-form size effect equation is not possible. It was shown that the size effect on the standard deviation can be approximated by an equation similar to Eq. (11) [60], i.e.,

$$\delta_{\psi_c} = \delta_0\left[\frac{n_3}{n} + \left(\frac{n_4}{n}\right)^{v/m}\right]^{1/v} \tag{12}$$

where δ_0, n_3, n_4, v =constants, which can also be determined from the distribution function $P_1(\psi)$ [60]. Based on Eqs. (11) and (12), we can calculate the size effect on the coefficient of variation (CoV). It is clear that, for large values of n, the CoV of ψ_c approaches a constant, which is a salient feature of the Weibull distribution.

It is evident that the finite weakest-link model is anchored by a discrete description of spatial randomness of resistance for individual potential localization zones. As discussed, the model assumes that the random resistances, ψ_i $(i = 1, \ldots, n)$ in Eq. (1), for the localization onset at individual possible locations, are statistically independent from each other. Therefore, the details of the

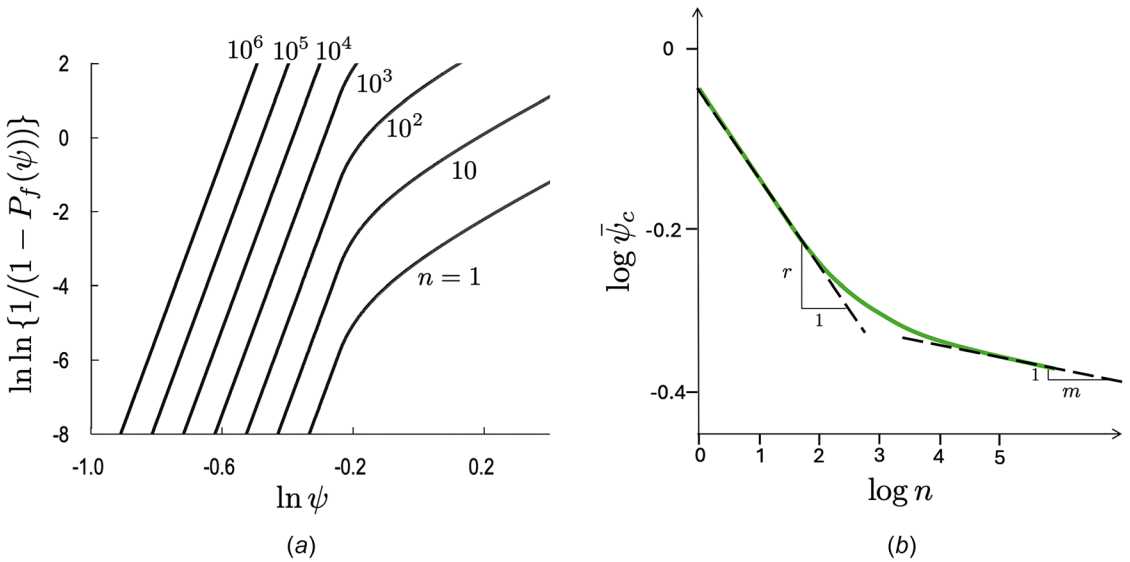

Fig. 2 Scaling of the probability distribution of structural resistance: (*a*) size effect on the distribution function, and (*b*) size effect on the mean resistance

spatial correlation of resistance are not considered in the model. This implies that the size of localization zone must be considerably larger than the correlation length of spatial distribution of resistance. To remove this constraint, we need to directly consider the possible spatial correlation among the random resistances ψ_i's. This leads to the development of the level excursion model, which will be discussed next.

2.2 Level Excursion Model. The spatial correlated resistances corresponding to the formation of the individual localization zone at different locations can be mathematically represented by a random field $\psi_l(\boldsymbol{x})$. The random field is characterized by the cdf of ψ_l, denoted by $F_{\psi_l}(\psi)$, at a local point together with an autocovariance function. It is important to note that the random value of ψ_l at location $\boldsymbol{x}$ refers to the resistance of the structure if the localization zone is centered at $\boldsymbol{x}$. The autocovariance function involves a length scale ℓ, commonly referred to as the correlation length, which measures the distance between two points at which the correlation essentially vanishes. It should be noted that the length scale ℓ is intimately related to the size of the localization zone as well as the correlation length of local material resistance [49,51].

By modeling the structural resistances for different potential localization zones as a random field $\psi_l(\boldsymbol{x})$, the cdf of overall structural resistance can be written by

$$P_f(\psi) = \Pr\left\{\sup_{x\in\Omega} -\psi_l(\boldsymbol{x}) \geq -\psi\right\} \tag{13}$$

where Ω denotes the structure domain. Consider the case where $\psi_l(\boldsymbol{x})$ is a homogenous random field, we can decompose $\psi_l(\boldsymbol{x})$ by $\psi_l(\boldsymbol{x}) = \bar{\psi}_0 + \delta\psi(\boldsymbol{x})$, where $\bar{\psi}_0$ = mean value of ψ and $\delta\psi(\boldsymbol{x})$ = zero-mean homogenous random field. Equation (13) becomes

$$P_f(\psi) = 1 - \Pr[\varphi(\boldsymbol{x}) \leq \lambda(\psi),\ \forall \boldsymbol{x} \in \Omega] \tag{14}$$

where $\varphi(\boldsymbol{x}) = -\delta\psi(\boldsymbol{x})$ and $\lambda(\psi) = \bar{\psi}_0 - \psi$. Evidently, the cdf of structural resistance is equal to the probability that the random field $\varphi(\boldsymbol{x})$ up-crosses a barrier $\lambda(\psi)$ at least once (Fig. 3). A common approach is to consider the case of the high barrier, where the individual crossing events are treated to be statistically independent [54,61,62]. In this case, the upcrossing events can be modeled by a Poisson counting process. The noncrossing probability can then be expressed by [54,62]

$$\Pr[\varphi(\boldsymbol{x}) \leq \lambda(\psi),\ \forall \boldsymbol{x} \in \Omega] = F_\varphi(\lambda)\exp\left[-\frac{\mu(\lambda)}{F_\varphi(\lambda)}V_\Omega\right] \tag{15}$$

where $\mu(\lambda)$ = mean crossing rate, and $F_\varphi(x)$ = cdf of φ. The prefactor $F_\varphi(x)$ represents the noncrossing probability (survival probability) at the starting point. By substituting Eq. (15) with Eq. (13), we have

$$P_f(\psi) = 1 - F_\varphi(\lambda)\exp\left[-\frac{\mu(\lambda)}{F_\varphi(\lambda)}V_\Omega\right] \tag{16}$$

To calculate the mean crossing rate, we first transform the random field $\varphi(\boldsymbol{x})$ to an equivalent Gaussian field $\varphi_G(\boldsymbol{x})$ [63,64]. Random fields $\varphi_G(\boldsymbol{x})$ and $\varphi_G(\boldsymbol{x})$ are related through their cdfs and autocovariance functions

$$\varphi_G(\boldsymbol{x}) = \Phi^{-1}\{F_\varphi[\varphi(\boldsymbol{x})]\} \tag{17}$$

$$R_F(|\Delta\boldsymbol{x}|) = \int_{-\infty}^{+\infty}\cdots\int_{-\infty}^{+\infty}\phi\{y_1,\ldots,y_{n_d},R_G(|\Delta\boldsymbol{x}|)\}\prod_i^{n_d}\left(F_\varphi^{-1}[\Phi(y_i)]\right)\mathrm{d}y_1\cdots\mathrm{d}y_{n_d} \tag{18}$$

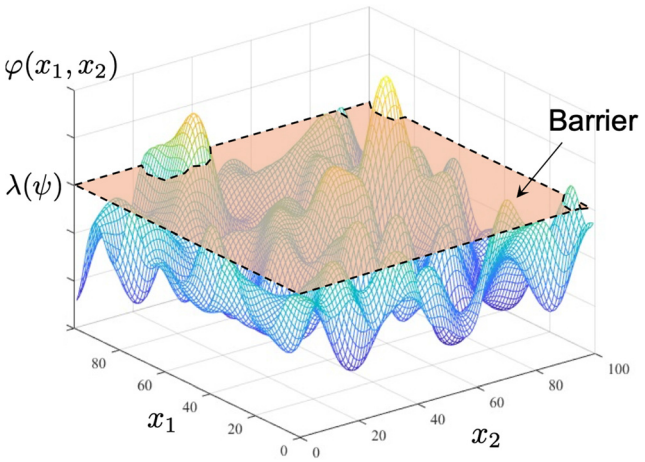

Fig. 3 Level excursion model in two-dimensional

where $\Phi(x)$ = standard Gaussian cdf, $\phi(\cdot)$ = joint Gaussian probability density function (pdf), $R_F(|\Delta \boldsymbol{x}|)$ and $R_G(|\Delta \boldsymbol{x}|)$ are the autocovariance functions of the random fields $\varphi(\boldsymbol{x})$ and $\varphi_G(\boldsymbol{x})$, respectively, $|\Delta \boldsymbol{x}|$ = distance between any two points, and n_d = dimensionality of the problem. It should be noted that it is not always possible to find an autocovariance function of the equivalent Gaussian field that would give the target autocovariance function for the original field. It has been shown that the target autocovariation function needs to satisfy certain requirements for Eq. (18) to have a non-negative definite solution of $R_G(|\Delta \boldsymbol{x}|)$ [64]. Based on this transformation, the original crossing barrier is transformed for the corresponding Gaussian field, i.e., $\lambda_Y = \Phi^{-1}[F_\varphi(\lambda)]$.

The mean crossing rate for an n_d-dimensional stationary Gaussian field has been extensively investigated [54,65,66]. The crossing rate is interpreted as the expected number of local maxima of the field above the barrier λ_Y per unit size of the domain. Therefore, the mean crossing rate can be related to the differential topology characteristic of the excursion set, i.e., the part of the random field $\varphi_G(\boldsymbol{x})$ that protrudes the barrier. The differential topology characteristic is asymptotically equivalent to the Euler characteristic when the barrier becomes sufficiently high [65]. Accordingly, the mean crossing rate can be expressed by [66]

$$\mu(\lambda) \approx \frac{\exp\left(-\lambda_Y^2/2\right)(\det \Lambda)^{1/2}}{(2\pi)^{(n_d+1)/2}} H_{n_d-1}(\lambda_Y) \tag{19}$$

where Λ = the covariance matrix of the spatial gradient of the random field $\varphi_G(\boldsymbol{x})$, and $H_k(x)$ = the kth Hermite polynomial, which can be written as

$$H_k(x) = k! \sum_{j=0}^{k} \frac{(-1)^j x^{(k-2j)}}{j!(k-2j)!2^j} \tag{20}$$

The covariance matrix Λ can be calculated directly from the power spectral density function of $\varphi_G(\boldsymbol{x})$

$$\Lambda_{ij} = \int_0^{+\infty} \ldots \int_0^{+\infty} \omega_i \omega_j G_Y(|\boldsymbol{\omega}|) \mathrm{d}\omega_1 \cdots \mathrm{d}\omega_{n_d} \tag{21}$$

where $|\boldsymbol{\omega}| = \sqrt{\sum_{i=1}^{n_d} \omega_i^2}$, and $G_Y(|\boldsymbol{\omega}|)$ is the one-sided power spectral density function of $\varphi_G(\boldsymbol{x})$. For an n-dimensional isotropic random field, $G_Y(|\boldsymbol{\omega}|)$ and $R_Y(|\Delta \boldsymbol{x}|)$ can be further related as [67–69]

$$G_Y(|\boldsymbol{\omega}|) = \int_0^{\infty} |\boldsymbol{\omega}| J_v(\eta|\boldsymbol{\omega}|) R_G(\eta) \left(\frac{2\eta}{\pi|\boldsymbol{\omega}|}\right)^{n_d/2} \mathrm{d}\eta \tag{22}$$

where

$$J_v(x) = \frac{(x/2)^\nu}{\sqrt{\pi}\Gamma(\nu + 0.5)} \int_0^{\pi} \cos(x\cos\theta)(\sin\theta)^{2\nu} \mathrm{d}\theta \tag{23}$$

which is the Bessel function of the first kind of order ν, and $\nu = n_d/2 - 1$.

Similar to the finite weakest-link model, the level excursion model predicts an intricate size effect on the probability distribution of structural resistance, and consequently a mean size effect. An important feature of the level excursion model is that it allows for the construction of the small-size asymptotic behavior of the size effect on the mean resistance. Because of the spatial correlation of the random field, the model predicts a vanishing size effect on the mean structural resistance at the small-size limit [49]. At the large-size limit ($V_\Omega \to \infty$), Eq. (17) indicates that the entire cdf of ψ is governed by high barrier (i.e., large values of λ or equivalently small values ψ). By noting $F_\varphi(\lambda) = 1 - F_{\psi_l}(\psi)$ and considering small values of ψ, Eq. (17) becomes $P_f(\psi) \approx 1 - \exp\{-\mu(\lambda)V_\Omega\}$. Recent studies showed that, if $F_{\psi_l}(\psi)$ has a power-law tail $F_{\psi_l}(\psi) \propto \psi^m$, the mean crossing rate would also exhibit a power-law behavior in terms of ψ, i.e., $\mu(\lambda) \propto \psi^m$. Therefore, we conclude that, at the large-size limit, the level excursion model would predict a Weibull distribution of ψ, and a Weibull size effect on the mean resistance. This result is well expected because the level excursion model represents a continuum generalization of the weakest-link model. We may divide the structure domain into a number of subdomains. If the size of each subdomain is chosen to be considerably larger than the correlation length of the random field $\psi_l(\boldsymbol{x})$, then the minimum resistances of individual subdomains can be treated as statistically independent from each other. Therefore, the cdf of overall structural resistance can then be calculated by using the finite weakest-link model, where each element in the chain represents a subdomain. The large-size asymptotic behavior of the level excursion model must be the same as that of the finite weakest-link model.

Figure 4(*a*) shows the typical size effect curve on the mean structural resistance predicted by the level excursion model. As discussed, the resulting mean size effect curve is very similar to that predicted by the finite weakest-link model for intermediate and large size regimes. For small-size regime, the level excursion model is able to reach zero-size limit. By contrast, the minimum structure size that the weakest-link model can handle is the size of a single localization zone. By using asymptotic matching, the mean size effect curve on structural resistance predicted by the level excursion model can be approximated by [49]

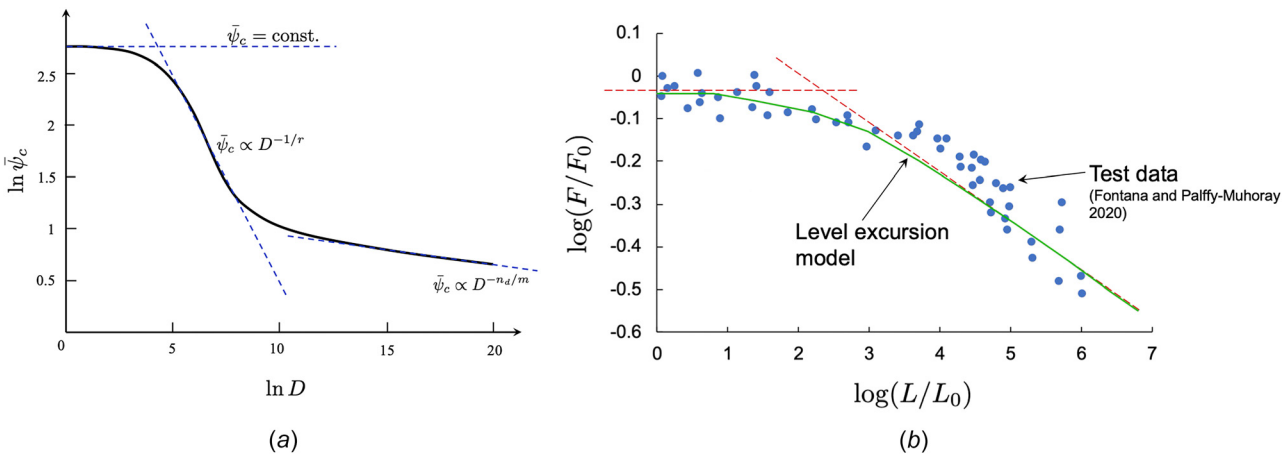

Fig. 4 (*a*) Mean size effect curve of the structural resistance predicted by the level excursion model and (*b*) comparison with the measured size effect on the fiber strength [70]

$$\bar{\psi}_c = \psi_0 \left\{ \frac{D_1}{D + D_1} + \left(\frac{D_2}{D + D_1} \right)^{\frac{r}{n_d m}} \right\}^{1/r} \tag{24}$$

where D = characteristic structure size, ψ_0, D_1, D_2, r = constants. Constant D_1 is of the order of the correlation length of the random field $\psi_l(\boldsymbol{x})$ [49].

2.3 Statistical Size Effect. It is clear that both the finite weakest-link model and the level excursion model predict that, for the case where the structure features a localization-induced failure and the location of localization onset is random, the probability distribution of structural resistance is strongly dependent on the structure size. This dependence leads to size effects on the mean resistance as well as on the higher-order statistical moments of structural resistance. The resulting mean size effect (Eq. (24)), commonly referred to as the statistical size effect, is particularly interesting. As mentioned earlier, this size effect is exactly what da Vinci speculated with regard to the length effect on rope strength. In a recent experiment, the tensile strengths of polyester and polyamide fibers of different lengths (from 1 mm to 1 km) were investigated [70]. As shown in Fig. 4(*b*), this experimental result clearly demonstrated a statistical size effect, which can be well fitted by Eq. (24).

The essential point here is that this size effect arises from the spatial randomness of the onset of localization. Therefore, such a mean behavior is of pure statistical nature, which is a unique feature of localization-induced failures. Clearly, the statistical size effect would be absent if the location of localization onset is predetermined. One common example in structural mechanics is structures with a pre-existing crack. In this case, due to stress concentration the localization zone must form at the crack tip and, therefore, such structures would not exhibit any statistical size effect [35,71]. As will be discussed in the subsequent sections, understanding the probabilistic behavior of localization-induced failures is of critical importance for the interpretation of experimental results as well as for the reliability-based structural design.

3 Strength Distribution of Quasi-Brittle Structures

3.1 Finite Weakest-Link Model of Strength Distribution. One of the most important design considerations for load-bearing structures is the peak load capacity. Many engineering structures are made of quasi-brittle materials, which include concrete, composites, ceramics, rock, cold asphalt, etc. In various engineering applications, these materials often exhibit a strain-softening behavior leading to damage localization. For the analysis of scaling behavior, it is convenient to express the peak load capacity, $P_{\max}$, of the structure in terms of the nominal strength, which is defined by $\sigma_N = P_{\max}/bD$ (D = characteristic size of the structure, and b = width of the structure in the transverse direction). For many commonly used geometries for laboratory testing, such as flexural specimens under three-point or four-point bending and tension specimens, the peak load is attained once a localized damage zone is fully formed, which is typically accompanied by the initiation of a macrocrack. Due to material heterogeneity, the local material strength is random, and therefore the location of the onset of localization damage is uncertain. The finite weakest-link model provides a sound mathematical tool to model the strength distribution of these quasi-brittle structures. In this case, the overall structural resistance ψ_c in Eq. (1) corresponds to the nominal structural strength σ_N. We may discretize the structure into a number of representative material elements, where each element represents a potential localization zone. Since in general the structure experiences a nonuniform stress field, we modify Eq. (2) to capture this behavior, i.e.,

$$P_f(\sigma) = \Pr(\sigma_N \le \sigma) = 1 - \prod_{i=1}^{n} [1 - P_1(s_i \sigma)] \tag{25}$$

where s_i = constants such that $s_i\sigma$ is equal to the maximum principal stress for element i. When the structure is considerably larger than the representative material element, Eq. (25) can be rewritten in an integral form

$$P_f(\sigma) = 1 - \exp\left\{ \frac{1}{V_0} \int_\Omega \ln\{1 - P_1[s(\boldsymbol{x})\sigma]\} \mathrm{d}V(\boldsymbol{x}) \right\} \tag{26}$$

where V_0 = volume of the representative material element, and $s(\boldsymbol{x})$ = stress field such that $s(\boldsymbol{x})\sigma$ = the maximum principal stress at point $\boldsymbol{x}$. From Eqs. (10*a*), (10*b*), and (25), it is clear that, for small values of σ, the cdf of σ_N can be modeled by a chain of elements with a power-law strength distribution, which leads to a Weibull distribution. For the rest portion of the cdf, it would follow a chain of Gaussian elements. As the structure size increases, $P_f(\sigma)$ is governed more dominantly by small values of σ, and therefore the Weibullian portion would occupy a larger portion of $P_f(\sigma)$. Eventually, for very large-size structures, the entire distribution function becomes Weibullian.

Figure 5 shows the experimentally measured strength distributions of specimens made of different engineering ceramics [72–74] and their optimum fits by Eq. (26). It is seen that, on the Weibull scale, the probability distributions of the nominal strength do not follow a straight line. At low stresses the distribution follows a Weibull distribution whereas it deviates from the Weibullian behavior in the intermediate and high probability regimes. The underlying reason is that, in most cases, the laboratory test specimens are not sufficiently large as compared to the size of the representative material element. Therefore, the resulting distribution function of the nominal strength does not belong to the class of extreme value statistics and it would necessarily deviate from the Weibull distribution. By accounting for the non-negligible size of the representative material element, the finite weakest-link model is able to provide optimum fits of these strength distributions.

As discussed earlier, the most important prediction of the finite weakest-link model is the size dependence of the strength statistics. A recent experiment on the low-temperature flexural failure of asphalt mixture beams has demonstrated this size effect [59]. Figure 6 shows the measured strength distributions of geometrically similar beams of two different sizes under three-point bending. A clear size effect on the strength distribution is observed. It is seen from Fig. 6 that, as the beams size increases, the lower Weibull portion of the distribution function becomes more dominant. Note that the slopes of the Weibull portions of these two specimen sizes are the same, which indicates that the Weibull modulus is independent of the structure size. With one set of model parameters, the finite weakest-link model can fit both strength distributions, which demonstrates its ability of capturing the size effect on the strength distribution.

3.2 Level Excursion Model of Failure of Polycrystalline Silicon Micro-Electromechanical Systems Devices. In addition to conventional macroscopic engineering materials, there is also a surging interest in understanding the strength distribution of microscale structures and devices, such as the micro-electromechanical systems (MEMS) structures. Over the last two decades, significant advances have been made in experimental testing of MEMS structures, which led to an improved knowledge of their probabilistic failure behaviors. The recent development of the on-chip testing device and slack-chain tester allows the measurements of the statistics of the tensile strength of polycrystalline silicon (poly-Si) MEMS structures [75,76]. Experiments showed that the sidewall of poly-Si MEMS specimens has surface grooves, which can be characterized as a set of V-notches with random spacings and geometries (Figs. 7(*a*) and 7(*b*)). The randomness of the sidewall geometry inevitably leads to a random stress field for a given applied load. The existence of the sidewall grooves indicates that the localized failure must occur somewhere along the sidewalls.

In a recent study [49], a level excursion model was developed to capture the random stress field and random material strength jointly. By employing a continuum description of failure behavior, the

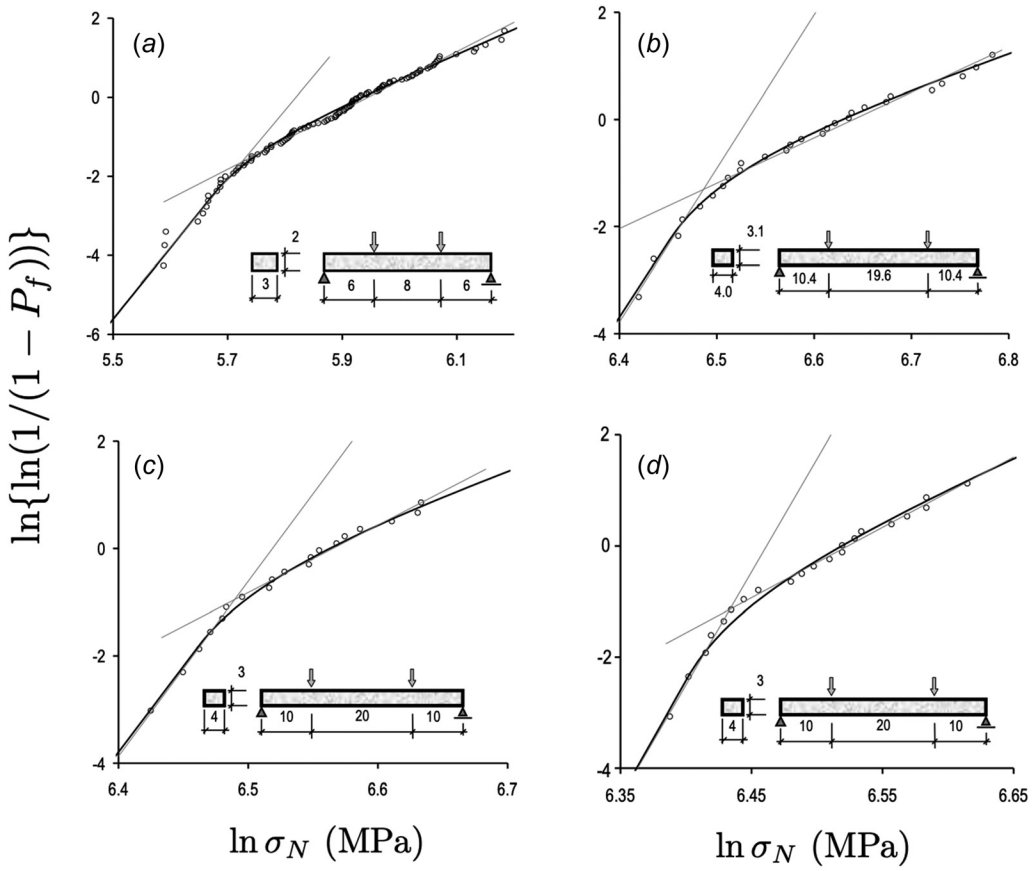

Fig. 5 Measured strength distributions of quasi-brittle structures and their optimum fits by the weakest-link model: (*a*) sintered α−silicon carbide (SiC) ceramics [72], (*b*) silicon nitride ceramics (Si_3N_4) [73], (*c*) Si_3N_4 with sintering additive (Si_3N_4–Al_2O_3–Y_2O_3) [74], and (*d*) Si_3N_4 with aluminum additive (Si_3N_4–Al_2O_3–CTR_2O_3) [74] (all dimensions are in mm)

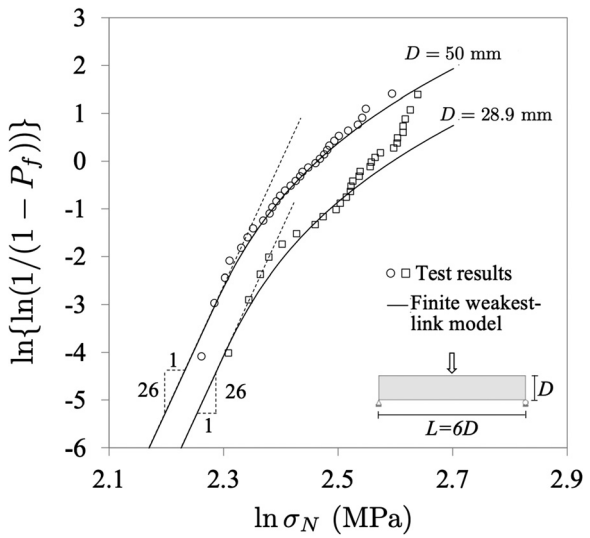

Fig. 6 Measured size effect on the strength distribution of flexural specimens made of cold asphalt mixtures

model uses a nonlocal failure criterion. It states that localization zone forms when the nonlocal tensile stress is greater than the local material tensile strength, i.e.,

$$\bar{\sigma}(x) = \int_{\Omega} \alpha(x - x')\sigma_1(x', y)\mathrm{d}x'\mathrm{d}y \geq f_t(x) \tag{27}$$

where

$$\alpha(x - x') = l_y^{-1}\left[1 - \left(\frac{16}{15}\right)^2 \frac{|x - x'|^2}{l_x^2}\right]^2 \tag{28}$$

$\sigma_1(x', y)$ = maximum principal stress at location (x', y), l_x, l_y = length constants, and Ω = nonlocal averaging zone, which is defined by a rectangular strip of width l_y along the entire sidewall. The nonlocality of the failure criterion physically captures the finite size of the fracture process zone formed at the incipient of localization failure. Evidently, the nonlocal stress field is proportional to the applied far-field tensile loading σ_N, i.e., $\bar{\sigma}(x) = \sigma_N z(x)$. Due to the random sidewall geometry, $z(x)$ can be modeled as a random field. Meanwhile, the spatially random local tensile strength can also be represented by a random field $f_t(x)$. Since the peak load of the specimen is attained once one localization zone is formed at the sidewall, the failure probability of the specimen under tensile loading σ_N can be expressed by

$$P_f(\sigma_N) = 1 - \Pr[\sigma_N z(x) \leq f_t(x),\ \forall x \in L_w] \tag{29}$$

where L_w denotes the sidewalls of the specimen. By considering that $z(x)$ and $f_t(x)$ are homogenous random fields and decomposing them into their mean values (μ_z, μ_{f_t}) and the corresponding zero-mean random fields $(z_0(x), \tilde{f}_t(x))$, i.e., $z(x) = \mu_z + z_0(x)$ and $f_t(x) = \mu_{f_t} + \tilde{f}_t(x)$, Eq. (29) can be rewritten by

$$P_f(\sigma_N) = 1 - \Pr[\eta_0(x) \leq \lambda,\ \forall x \in L_w] \tag{30}$$

where $\eta_0(x) = \sigma_N z_0(x) - \tilde{f}_t(x)$ and $\lambda = \mu_{f_t} - \sigma_N \mu_z$.

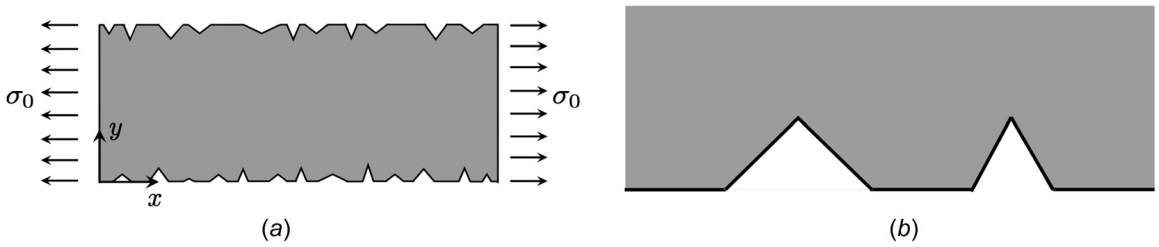

Fig. 7 (*a*) Schematic of uniaxial tensile test on poly-Si MEMS specimens and (*b*) zoom-in view of the sidewall geometry

Since this is a one-dimensional (1D) problem, Eq. (19) reduces to the classical result of Rice's 1D crossing rate [77], where the mean crossing rate is given by $\mu_\lambda = \mathbb{E}[\dot{\eta}(x)^+|\eta_0(x)=\lambda] = \int_0^\infty \zeta f_{\eta\dot{\eta}}(\lambda,\zeta)\mathrm{d}\zeta$, where $\mathbb{E}(\cdot)$ = expectation operator, superscript "+" denotes the positive gradient, $\dot{\eta}(x) = \mathrm{d}\eta(x)/\mathrm{d}x$, $f_{\eta\dot{\eta}}(\cdot,\cdot)$ = joint probability density function (pdf) of η and $\dot{\eta}$. Based on Eqs. (16)–(19), we first transform $\eta_0(x)$ to an equivalent standard Gaussian field $\varphi_G(x)$, and the mean crossing rate can be estimated by

$$\mu_\lambda \approx \frac{\delta_{\dot{\varphi}_G}}{\sqrt{2\pi}}\phi_G(\lambda_G) \tag{31}$$

where $\phi_G(y)$ = pdf of standard Gaussian distribution, $\lambda_G = \Phi^{-1}[F_{\eta_0}(\lambda)]$, and $\delta_{\dot{\varphi}_G}$ = standard deviation of the spatial derivation of the equivalent Gaussian field $\mathrm{d}\varphi_G/\mathrm{d}x$. Note that $\delta_{\dot{\varphi}_G}$ can be directly calculated from the power spectral density of $\varphi_G(x)$: $\delta_{\dot{\varphi}_G} = \sqrt{\int_{-\infty}^{\infty}\omega^2 S_{\varphi_G}(\omega)\mathrm{d}\omega}$, where $S_{\varphi_G}(\omega)$ = power spectral density of $\varphi_G(x)$. Based on Eqs. (16), (30), and (31), the failure probability of the uniaxial tensile MEMS specimen can be calculated by

$$P_f(\sigma_N) = 1 - F_{\eta_0}(\lambda)\exp\left\{-\sqrt{\frac{2}{\pi}}\frac{\delta_{\dot{\varphi}_G}}{F_{\eta_0}(\lambda)}\phi_G(\lambda_G)L\right\} \tag{32}$$

where L = specimen length.

Based on the measurements of the sidewall geometry [76], the random sidewall geometry is characterized by the probability distributions of the spacing of V-notches, the notch angle, and the notch depth (see Ref. [49] for details). From these information, the random nonlocal stress field $z(x)$ can be determined from the Monte Carlo simulations of the random elastic stress field [49]. For the random field of local tensile strength $f_t(x)$, the cdf of local tensile strength is considered to follow a Gauss-Weibull distribution described by Eqs. (10*a*) and (10*b*), and the spatial correlation of local tensile strength is described by a squared exponential autocovariance function $R_{f_t}(\Delta x) = \delta_s^2 \exp[-(\Delta x/l_a)^2]$, where δ_s = standard deviation of f_t, Δx = distance between two points on the sidewall, and l_a = constant, which is of the order of the size of a single silicon grain. The cdf of f_t is calibrated through the optimum fitting of the measured strength distributions.

Figure 8 shows, on the Weibull scale, the optimum fitting of two sets of size effect tests on the strength distributions of poly-Si MEMS specimens by the level excursion model. The details of these tests can be found in Refs. [76] and [78]. It is seen that, with one set of parameters for the cdf of f_t, the model is able to capture the length effect on the strength distribution. Clearly, none of the specimens exhibits a strength distribution that can be fitted by a two-parameter Weibull distribution. Previous studies have suggested using three-parameter Weibull distribution, which gives an improved fitting as compared to the two-parameter Weibull model. However, the three-parameter Weibull distribution cannot provide optimum fits of the strength distributions of specimens of different sizes by using one set of parameters. This indicates that the Weibull modulus, scaling parameter, as well as the strength threshold, must be treated to be size dependent. The physical justification of such size dependence is lacking. Therefore, the three-parameter Weibull distribution remains as an empirical model, which cannot be used for prediction of strength distribution of MEMS specimens of different lengths.

The aforementioned analysis indicates the importance of the size-effect test of the strength distributions of specimens. In practice, experimental testing of strength distribution often involves a limited number of specimens, which covers only the central range of the probability. Consequently, in many cases, the measured strength distribution can be fitted by multiple distribution functions equally well. One effective means to distinguish the different choices of the distribution functions is to test the strength distributions of geometrically similar specimens of different sizes, because the correct probabilistic model must be able to capture the underlying statistical size effect on the structural strength. This is a new perspective on the experimental characterization of strength distribution of quasi-brittle structures, which is broadly applicable to the probability distribution of structural resistance associated with localization-induced failures.

4 Implications for Stochastic Finite Element Simulations of Quasi-Brittle Fracture

The foregoing discussion revolves around the statistical size effect on the strength distribution of quasi-brittle structures. It was recently found that this scaling behavior has important implications for stochastic FE simulations of damage and fracture of quasi-brittle structures [79–81]. To demonstrate it, let us consider a uniaxial tension specimen, where the material exhibits a bilinear stress–strain behavior. We divide the specimen into several elements along its length (Figs. 9(*a*) and 9(*b*)). According to the second law of thermodynamics, only one element will experience strain softening (damage), and the rest will undergo unloading [1,82]. For a given stress–strain relationship, the total energy dissipation of the specimen would vary with the element size. To ensure the objectivity of the simulation result, we need to adjust the postpeak tangential stiffness as a function of element size so that the total energy expended to completely damage an element is always equal to the energy dissipation for propagating a macrocrack throughout the element, which is the essential idea behind the crack band model [2,20]. This leads to the following relation: $\gamma = G_f/l_e$ where γ = area under the stress–strain curve, l_e = element length, and G_f = mode I fracture energy.

Now consider that the tensile strength f_t and fracture energy G_f of each element are random variables. As a demonstration, we consider that total bar length $L = 1$ m and cross-sectional area $A_e = 5 \times 10^{-4}$ m^2. Both f_t and G_f follow Gaussian distributions. It is assumed that these two properties are mutually independent, and each property is also statistically independent across different elements. We take $E = 20$ GPa, mean tensile strength = 2.4 MPa, mean fracture energy = 90 J/m^2, and the coefficients of variation of f_t and G_f = 7.5%. To calculate the load–displacement response, we impose the equilibrium condition, that is the stress σ_i in any element is equal to P/A_e, and calculate the end displacement by $\Delta = \sum_{i=1}^{n}\epsilon_i l_e$, where P = applied load, $n = L/l_e$, and ϵ_i = strain in element i. For each

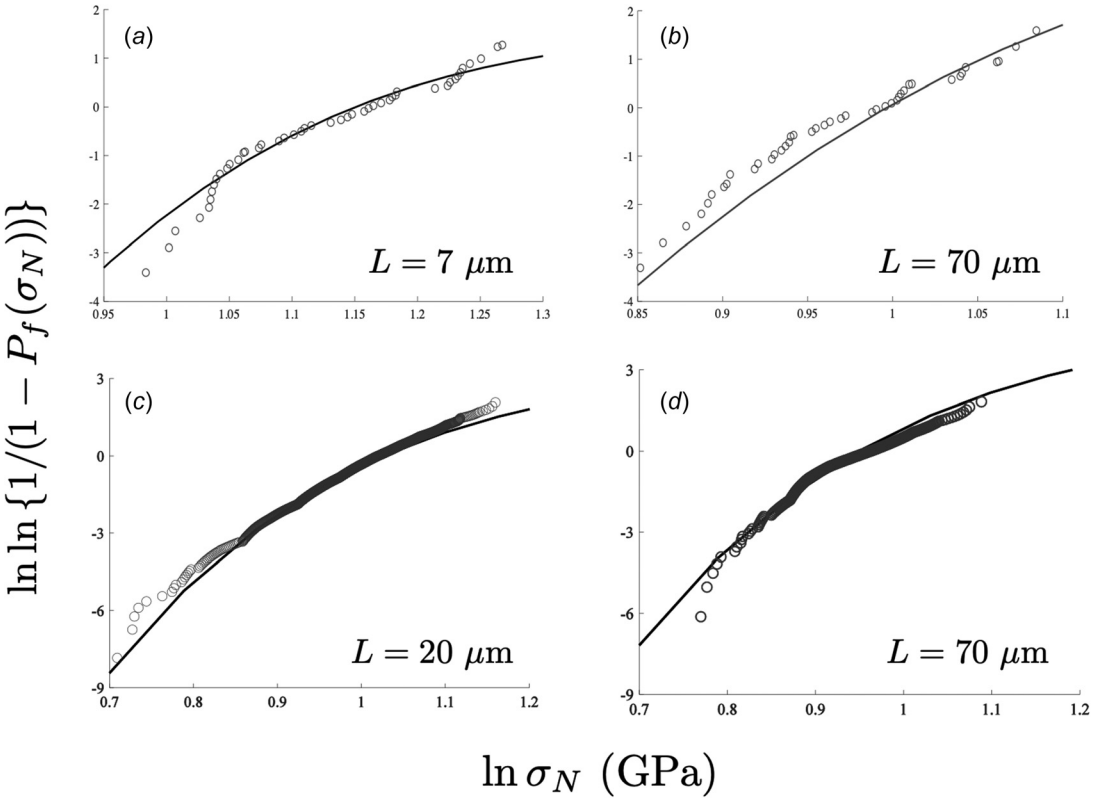

Fig. 8 Optimum fitting of the strength distributions of poly-Si MEMS specimens of different lengths by the level excursion model: (*a*) and (*b*) test data from Ref. [76], and (*c*) and (*d*) test data from Ref. [78]

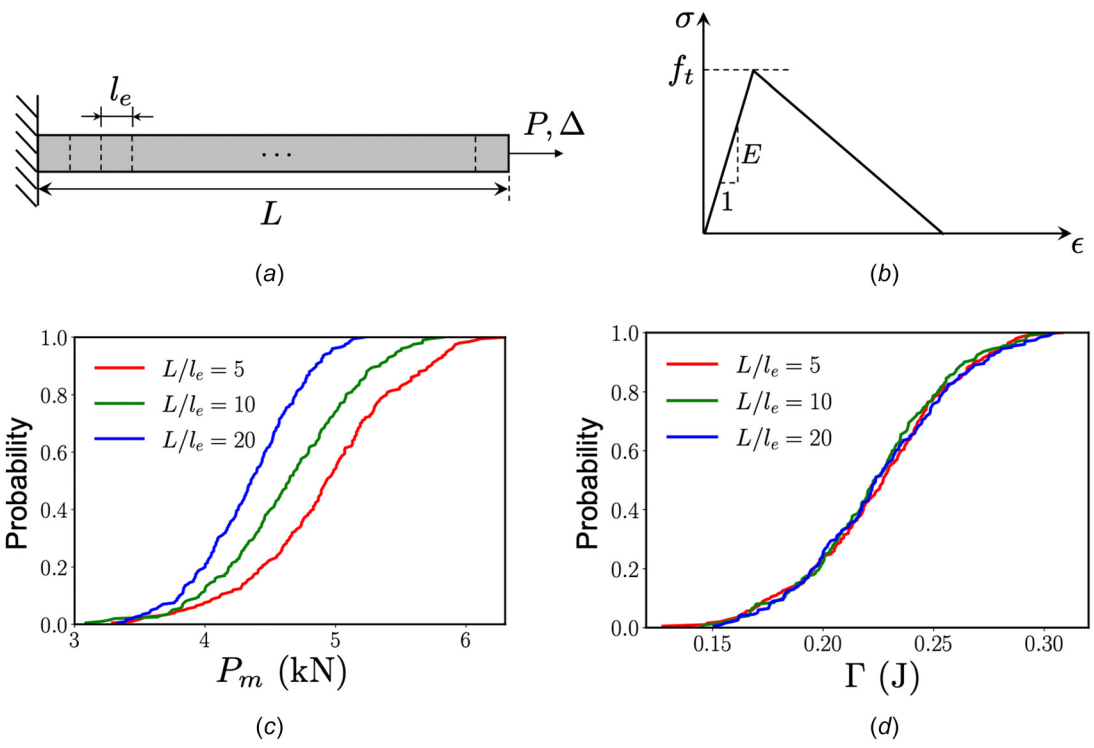

Fig. 9 Analysis of mechanical response of uniaxial tension specimen made of a strain-softening material: (*a*) problem setup, (*b*) stress–strain curve, (*c*) probability distribution of the peak load capacity, and (*d*) probability distribution of total energy dissipation of the bar

element, the postpeak portion of the stress–strain curve is adjusted based on the crack band model.

We consider three element sizes, $l_e = 50,\ 100,\ 200$ mm. For each case, a total of 200 realizations are used to calculate the stochastic response of the load–displacement curve. The interest here is to understand the dependence of the statistics of the peak load P_m and the total energy dissipation Γ of the bar on the discretization. It is evident that P_m is governed by the minimum strength of all the elements. Since the tensile strengths of the elements are statistically independent, the cdf of P_m can be calculated by the weakest-link model: $\Pr(P_m \le P) = 1 - [1 - P_1(P/A_e)]^n$, where $P_1(x) =$ strength cdf of a single element. Therefore, the cdf of P_m would depend on n, or equivalently on the element size l_e (Fig. 9(*c*)). On the other hand, based on the crack band model, the total energy dissipation Γ is equal to $A_e G_f$, which is independent of the element size (Fig. 9(*d*)).

The weakest-link model indicates that, in order to ensure a mesh-independent cdf of P_m, we must consider that the strength cdf $P_1(x)$ of a single element varies with the element size. This size dependence can be understood from the failure mechanism. Consider the element size is larger than the width of the damage localization zone l_0, a material characteristic length. If we further assume that the correlation length of material strength is less than l_0, $P_1(x)$ can be written by $P_1(x) = 1 - [1 - P_0(x)]^{n_e}$, where $n_e = l_e/l_0$ and $P_0(x) =$ strength cdf of a material element of size l_0. Evidently, the strength cdf $P_1(x)$ depends on the element size l_e. Substitution of the expression of $P_1(x)$ into the weakest-link model yields a mesh-independent prediction of the cdf of P_m.

The foregoing 1D analysis shows that the stochastic FE analysis of quasi-brittle fracture could still suffer spurious mesh sensitivity even if a proper energy regularization scheme is implemented. In addition to energy regularization, special cares are needed for the formulation of the probability distribution functions of constitutive properties of the finite element. For instance, in the aforementioned 1D example, the mesh dependence of the predicted probability distribution of peak load can be suppressed by considering a weakest-link model of the strength distribution of each single element, which reflects the localization mechanism. The essential point is that the probability distributions of the mechanical properties of the element need to be determined based on the element's mechanical behavior. For elements experiencing localized damage, the strength distribution would vary with the element size, a necessary consequence of the statistical scaling.

We can extend this concept to general stochastic FE analysis of quasi-brittle fracture. Consider that the spatial variation of random material properties are described by random fields. Recent studies have shown that indeed the mapping of random fields of material properties onto the FE meshes has profound implications for spurious mesh sensitivity in stochastic FE analysis [81]. The existing mapping methods include (1) the local projection, where the random value of the constitutive property of the finite element is set to the value of the corresponding random field at the centroid of the element, and (2) the local averaging, where the random value of the constitutive property is calculated by averaging of the corresponding random field over the domain covered by the finite element. When the FE mesh size is larger than the correlation length of material random field, neither of these approaches captures the statistical scaling of the strength property, and therefore they are not suitable for modeling the strength properties for the case of damage localization. As a consequence, these mapping methods lead to strong mesh dependence in the prediction of the high order statistical moments of the structural response [80,81].

Hinged by the notion that each finite element represents a material element of a finite size, a mechanistic mapping method was recently developed [81]. The method uses an adaptive approach, which directly relates the mapping method to the damage mechanism. It captures both the weakest-link effect for damage localization and the statistical averaging for distributed damage. The main consequence of the model is that the probability distribution functions of the constitutive properties of the finite element could depend on the element size, and the size dependence is dictated by the prevailing damage pattern. For localization-induced failures, which is common for quasi-brittle structures, this mesh size dependence of the probability distribution of strength properties essentially reflects the statistical scaling. Capturing the size dependence of the statistics of constitutive properties of the finite element plays an essential role in mitigating the spurious mesh sensitivity in stochastic FE simulations of quasi-brittle fracture.

5 Stochastic Shell Buckling

Shell buckling is a century old topic in structural mechanics. The salient feature of shell buckling is that the critical buckling pressure is highly sensitive to the initial geometric imperfection [83,84]. Due to the uncertainty in the manufacturing process, the profile of the initial geometric imperfection is inherently random, and consequently the buckling pressure of the shell is of statistical nature [85–88]. There has been an increasing interest in understanding the stochastic aspect of buckling of elastic spherical shells. There is abundant evidence that spherical shells exhibit a localized buckling behavior [89]. This localization phenomenon was theoretically studied for a perfect spherical shell by using the asymptotic expansion analysis of the initial post-buckling response [12]. For spherical shells with random geometric imperfections, the localized buckling zone could occur anywhere on the shell. As indicated by the mathematical framework presented in Sec. 2, the buckling pressure of shells would also exhibit a statistical scaling behavior.

Here we briefly review a recent study on the statistical scaling of the buckling pressure of clamped hemispherical shells with random geometric imperfections [39]. In this study, the imperfection was defined as the difference between the radial coordinate of a point on the shell surface and its nominal radius, and the thickness of the shell was kept constant. The amplitude of the geometric imperfections was modeled by a homogenous random field generated over the spherical surface (Fig. 10). For each realization of the geometric imperfections, the critical buckling pressure p_c of the shell was calculated by the finite element analysis. The probability distribution of p_c was determined by Monte Carlo simulations. For shell buckling, it is customary to express the critical buckling pressure in terms of the knockdown factor κ_c, which is defined by $\kappa_c = p_c/p_0$ where $p_0 =$ buckling pressure of a perfect hemispherical shell.

The simulation showed that, for a wide range of autocorrelation lengths, ℓ of the random imperfection amplitude, the average size A_b of the localized buckling zone is proportional to $R\sqrt{Rt}$, where $R =$ shell radius and $t =$ shell thickness [39]. Therefore, the number of potential buckling locations, N, over the entire hemispherical surface is proportional to $\sqrt{R/t}$. By considering that the buckling pressures for the formation of a buckling zone at different locations are statistically independent, the cdf of κ_c can be expressed by using the same form of Eq. (2), i.e., $P_f(\kappa) = \Pr(\kappa_c \le \kappa) = 1 - \prod_{i=1}^{N}[1 - P_{1i}(\kappa)]$, where $P_{1i}(\kappa)$ is the probability distribution of knockdown factor for the formation of a buckling zone at location i. Recent studies on spherical shells with dimple defects showed that regardless of the size of the dimple defects the critical buckling pressure would not fall below a threshold value κ_0 [36]. This implies that the distribution function $P_1(\kappa)$ must also exhibit a threshold behavior. By assuming that P_{1i}s have the same left tail distribution, the knockdown factor must approach a three-parameter Weibull distribution when R/t is very large.

For a given random distribution of geometric imperfections, the probability distribution function $P_1(\kappa)$ is also strongly influenced by the dimensionless radius R/t. Therefore, one cannot investigate the statistical scaling in shell buckling by simply changing R/t ratio. This is very different from the finite weakest-link model of strength statistics of quasi-brittle structures, in which the size of the localization zone is independent of the structure size. In a recent study [39], this statistical size effect was studied by changing the area of the shell surface that contains the geometric imperfections. In this way, one can change the number of potential locations of

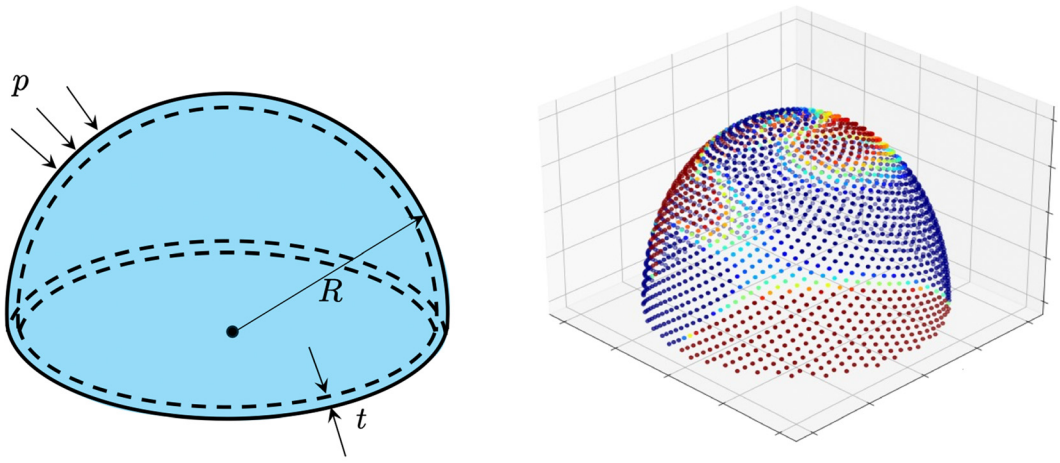

Fig. 10 Hemispherical shell under external pressure: (*a*) problem setup and (*b*) numerically generated random geometric imperfections

localized buckling while keeping a constant R/t (consequently $P_1(\kappa)$ is fixed).

Figure 11 presents the simulated probability distributions of critical buckling pressures of a hemispherical shell ($R = 20$ mm, $t = 0.2$ mm, $\ell = 0.12$ mm) with different areas A_I of the imperfection zone (the imperfection zone equals to whole, one half, one quarter, and one eighth of the hemispherical surface). To demonstrate the size effect on $P_f(\kappa)$, these distributions are plotted on a three-parameter Weibull paper, and the threshold is determined by optimum fitting of the probability distribution of κ_c for the case where the entire hemispherical surface contains imperfections. It is clear that, as the imperfection zone size gets smaller, the cdf of κ_c deviates considerably from a three-parameter Weibull distribution. With a decreasing number of potential buckling zones, the distribution of the knockdown factor would approach $P_1(\kappa)$, which cannot follow a Weibull distribution. Because if it did, $P_1(\kappa)$ would follow a weakest-link model indicating that the actual localized buckling zone would be much smaller.

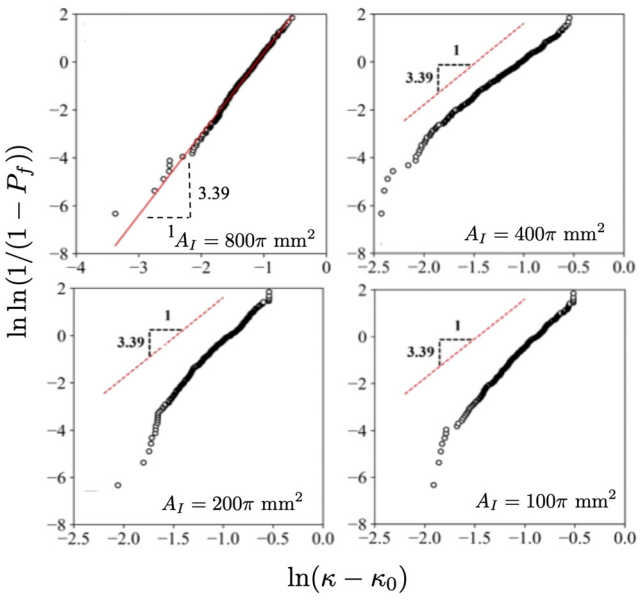

Fig. 11 Simulated probability distributions of the critical buckling pressure of shells with different sizes of the imperfection zone

Figure 12 shows that the mean buckling pressure decreases as the number of potential buckling locations, N, increases. Since the large-size asymptote of the cdf of critical buckling pressure follows a three-parameter Weibull distribution, the mean buckling pressure must approach the threshold pressure κ_0 as N becomes very large. The mean size effect on the buckling pressure can be described by an equation similar to Eq. (11)

$$\bar{\kappa}_c = \kappa_0\left(1 + \frac{N_0}{N}\right)^{1/r} \tag{33}$$

where $N_0, r =$ constants. It is seen from Fig. 12 that Eq. (33) fits the simulated mean size effect very well.

The aforementioned stochastic analysis revealed the dual role of dimensionless radius R/t in determining the knockdown factor of spherical shells: (1) it governs the deformation of the shell as predicted by the equilibrium equations of shell buckling, and (2) it dictates the statistical scaling of the buckling pressure. Previous researches in shell buckling has largely focused on deterministic analysis, and therefore the majority of our understanding of buckling of spherical shells pertains to the mechanistic role of R/t. By contrast, the statistical role of R/t (Eq. (33)) was discovered only lately [39]. This recent finding of statistical scaling in terms of R/t provides a new understanding of the buckling behavior of spherical shells with random geometric imperfections, and leads to a more complete perspective for interpretation of the experimental data on

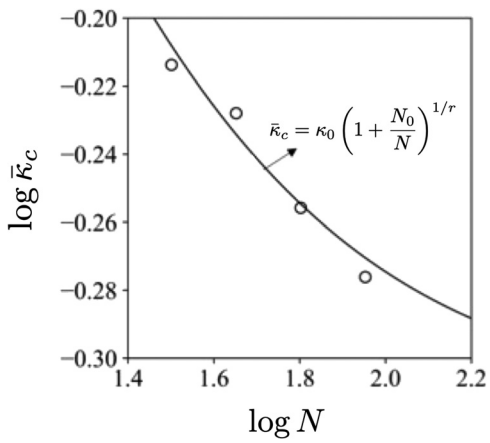

Fig. 12 Effect of the number of potential buckling locations on the mean buckling pressure

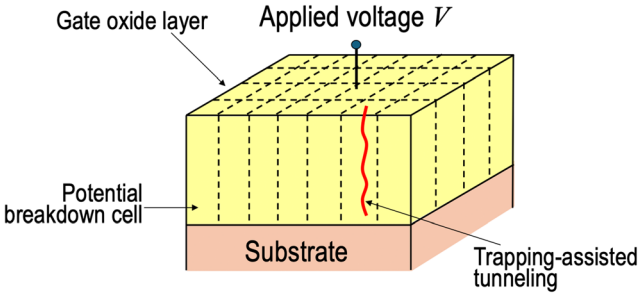

Fig. 13 Schematic of trapping-assisted breakdown mechanism of high–*k* gate dielectrics

shell buckling, which are often expressed in terms of the relationship between the buckling pressure and the dimensionless radius.

6 Electric Breakdown of High–*k* Gate Dielectrics

The preceding sections focus on structural failures under mechanical loading. The localization-induced failure also occurs in breakdown of electronic devices. Recent studies investigated the statistical scaling in electrical breakdown of high–*k* gate dielectrics under both DC and AC voltages [15,90]. In high–*k* gate dielectrics, electrons can be trapped in the gate oxide layer. When the trap density reaches a critical value, a weak localized path is formed between the gate electrode and the substrate. The Joule heating in the local breakdown path causes lateral propagation of the leakage spots, which eventually leads to a significantly increased tunneling current passing through the layer, commonly known as the hard breakdown.

To model the probability distribution of the breakdown voltage, we consider that the gate dielectric is composed of a number of cells (Fig. 13). The gate dielectric survives under the gate voltage if and only if all the cells are immune from the trapped-assisted tunneling process. The breakdown voltage of each cell is inherently random due to the randomness of the intrinsic defects. Therefore, the breakdown voltage V_g of the dielectric is equal to the minimum value of the breakdown voltages of all the cells. By considering the breakdown voltages of individual cells are statistically independent, the cdf of V_g can be calculated by using the weakest-link model (Eq. (2)), in which ψ represents the applied voltage. It has been shown that the breakdown voltage of an individual cell follows a Gauss-Weibull distribution (Eqs. 10(*a*) and 10(*b*)), with a grafting probability of the order of $10^{-10} - 10^{-8}$ [15]. It is clear that the breakdown voltage would exhibit a statistical scaling in terms of the gate area, as described by Eq. (11).

For the design of high–*k* gate dielectrics, one key consideration is the device lifetime t_f for a prescribed gate voltage V_0. To model the probability distribution of t_f, we need to use the relationship between the growth rate of the tunneling path and the applied voltage. By using the dielectric breakdown model, a power-law relation was proposed for the kinetics of the tunneling path, which yields $t_f V_0^{\varsigma} \propto V_g^{\varsigma+1}$ (ς = constant) [15]. With this relationship, one can derive the probability distribution function of device lifetime t_f from the cdf of V_g. It is clear that the statistics of device lifetime can also be described by a weakest-link model since the device lifetime is equal to the shortest lifetime of all the potential breakdown cells. The lifetime distribution of a single cell has a power-law tail, whose exponent is ς times smaller than that of the power-law tail of breakdown voltage distribution. The core of the lifetime distribution of the breakdown cell follows a Gaussian distribution transformed by a power-law function [15].

Figure 14 shows the optimum fitting of the measured lifetime distributions of high-*k* gate dielectrics by the finite weakest-link model as well as the two-parameter Weibull model. The model naturally predicts a strong dependence of the lifetime distribution on the gate area. Figure 15 shows the experimentally observed effect of gate area on the median lifetime, which compares well with the weakest-link model (solid curve in Fig. 15). Similar to the strength distribution of quasi-brittle structures (Fig. 5), the lifetime distribution of gate dielectrics deviates significantly from the two-parameter Weibull distribution. This deviation can be explained by the fact that, for these gate dielectrics tested, there is approximately 10^7 number of cells (the area of each cell is around 100 nm^2 and the gate area is about 10^{-3} mm^2). Since the power-law tail of the lifetime distribution of each cell only extends to a probability of the order of 10^{-8} or smaller, the lifetime distribution of the gate dielectrics cannot follow a Weibull distribution. As shown in Fig. 14, if one imposes a two-parameter Weibull distribution to fit the lifetime distribution, the design lifetime at low probabilities would be grossly underestimated.

7 Safety Factors for Reliability-Based Structural Design

The interest in stochastic analysis of failure of engineering structures is primarily motivated by the need for reliability-based design. The central idea of reliability-based design is to guard the structure against a tolerable failure probability P_c, which is typically on the order 10^{-6}. The overall failure probability P_F of the structure, which takes into account the randomness in both applied loads and structural resistance, can be calculated by

$$P_F = \int_0^{\infty} P_f(\psi) f_L(\psi) \mathrm{d}\psi \tag{34}$$

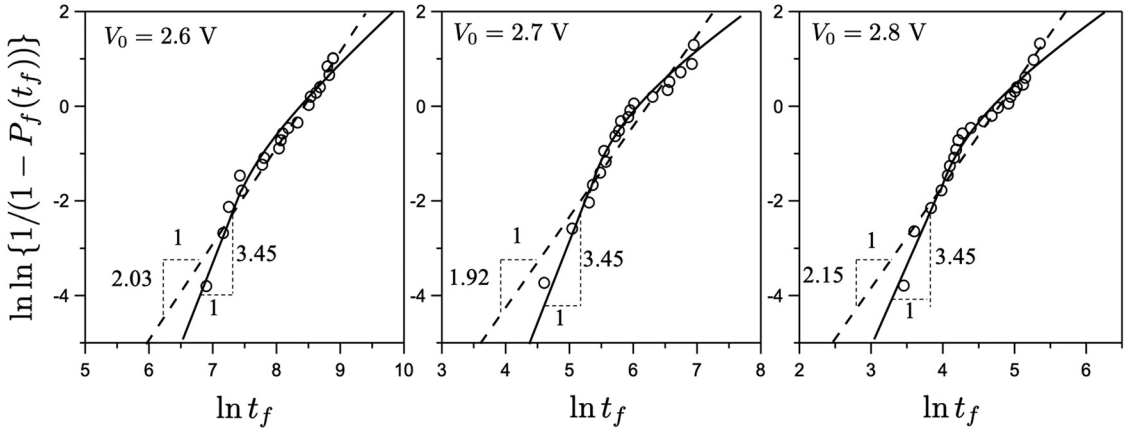

Fig. 14 Measured lifetime distributions of high–*k* gate dielectrics and their optimum fits by the weakest-link model and the two-parameter Weibull model

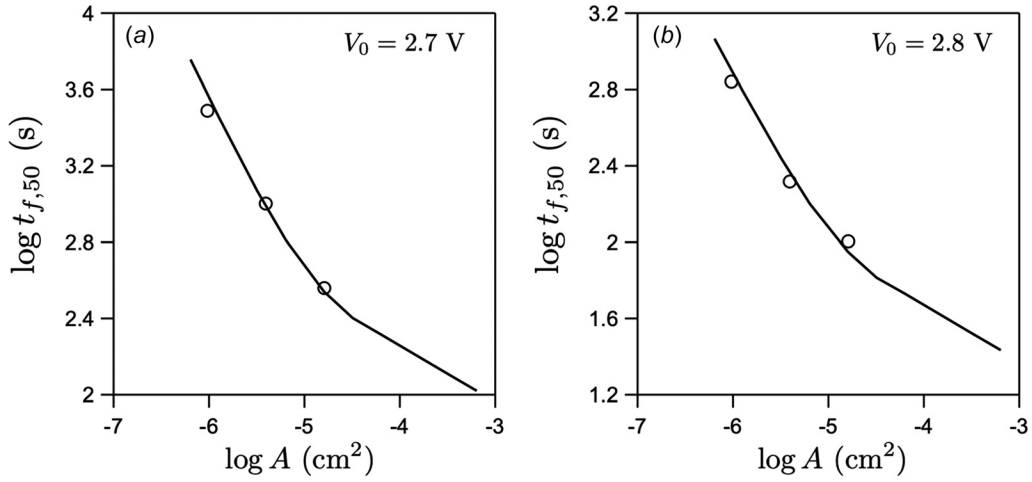

Fig. 15 Effect of the gate area on the median lifetime of high–*k* gate dielectrics under different applied voltages: (*a*) $V_0 = 2.7$ V and (*b*) $V_0 = 2.8$ V

where $f_L(\psi)$ = probability density function (pdf) of the applied load expressed in the same mathematical form as the structural resistance. As discussed in the preceding sections, for structures exhibiting localization-induced failures, the cdf of structural resistance $P_f(\psi)$ is strongly dependent on the structure size. Consequently, for a given structure geometry and applied loading, the overall failure probability P_F would vary with the structure size [60].

In reliability-based design, the direct use of Eq. (34) is cumbersome. One common approach is to use the safety factors, in which the failure state of the structure for a given failure probability P_c is described by

$$\bar{\psi}_c/\mu_L \le \bar{\zeta} \tag{35}$$

$$\text{or} \quad \frac{\bar{\psi}_c - k_R\delta_{\psi_c}}{\mu_L + k_L\delta_L} \le \zeta \tag{36}$$

where $\bar{\zeta}$, ζ are the central and nominal safety factors, respectively, k_L, k_R = constants, and μ_L, δ_L are the mean and standard deviation of the applied load, respectively. The underlying idea here is that the safety factors set the pdfs of resistance and applied load sufficiently apart from each other to guarantee a tolerable failure probability P_c (Fig. 16). The concept of safety factors is attractive in engineering practice because they only use the mean values and standard deviations of the structural resistance and the applied load.

It is evident that the safety factors ζ and $\bar{\zeta}$ must be determined to correspond to the target failure probability P_c. Since P_F is size dependent for localization-induced failures, it is expected that ζ and $\bar{\zeta}$ must also vary with the structure size. However, in almost all the existing design procedures for various engineering structures (e.g., reinforced concrete structures [91], nuclear claddings for light water reactors [92]), the safety factors are deemed independent of the structure size. This implies that, for the same geometry, structures of different sizes are designed for different levels of failure probability. Neglecting the size effect on safety factors can cause the structure to have a failure probability that is orders of magnitude higher than the targeted value [34,60].

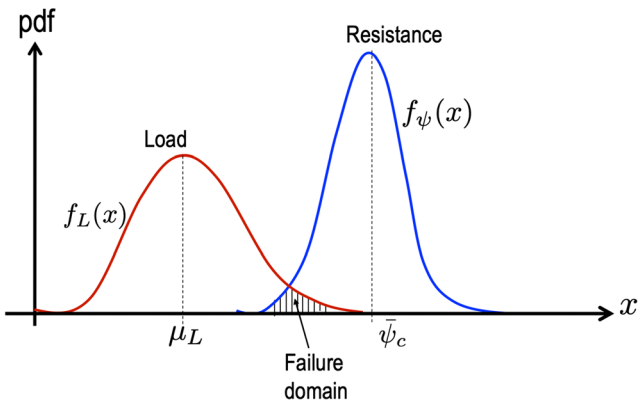

Fig. 16 Concept of safety factors for reliability-based structural design

Approximate size effect equations for the central and nominal safety factors were recently proposed for the case where the probability distribution of the applied load is nearly Gaussian [60]. These size effect models were derived by matching the small- and large-size asymptotes. At the small-size limit, both the applied load and the structural resistance follow a nearly Gaussian distribution. The far-left power-law tail of resistance distribution contributes minimally to the failure probability [60]. In this case, the failure probability P_F can be reasonably estimated by using the Cornell reliability index [93,94], from which the central safety factor can be expressed by

$$\bar{\zeta} = \frac{C_1}{1 - C_2\beta_c\omega_R(D)} \tag{37}$$

where C_1, C_2 = constants, $\beta_c = \Phi^{-1}(P_c)$ = critical value of the Cornell index for the failure probability P_c, and ω_R = CoV of structural resistance, which is size dependent. The expression of $\omega_R(D)$ can directly be obtained from Eqs. (11) and (12).

At the large-size limit, the structural resistance follows the Weibull distribution which is essentially a power-law function for the low probability regime ($P_f(\psi) \le 10\%$). Since the target failure probability P_c is low, we can use the power-law function for $P_f(\psi)$ in Eq. (34), i.e., $P_c = \int_0^\infty f_L(\psi)(\psi/S)^m d\psi$, from which we can solve the Weibull scaling parameter S for a given P_c value. The key point here is that parameter S is independent of structure size, and therefore the corresponding mean structural resistance must also be size-independent. What it follows is that, at the large-size limit, the safety factors must be size-independent.

Based on the foregoing analysis of the small- and large-size asymptotes, the size effects on the central and nominal safety factors can be approximated by the following equations [60]:

$$\bar{\zeta} = C_1[1 + C_2\gamma\beta_c\omega_R(D)]^{1/\gamma} \tag{38}$$

$$\zeta = \bar{\zeta}\left(\frac{1 - k_R\omega_R(D)}{1 + k_L\omega_L}\right) \tag{39}$$

where γ = constant, and ω_L = CoV of the applied load. Equations (38) and (39) indicate that the size effect on the safety factors is governed by the size effect on the CoV of structural resistance. For the case where the applied load is non-Gaussian, the forms of Eqs. (37) and (38) are still applicable except that one would need to replace the Cornell index by the Hasofer–Lind index [94].

8 Conclusions and Outlook

The probability distribution of the resistance of engineering structures and devices that exhibit localization-induced failures can be mathematically treated by the finite weakest-link model in a discrete framework and the level excursion model in a continuum framework. These mathematical models provide analytical expressions for the probability distribution of structural resistance, and offer a quantitative description of the statistical size effect on the structural resistance. Approximate equations have been developed for the size effects on the mean and standard deviation of structural resistance. Both the finite weakest-link model and the level excursion model have successfully been applied to a variety of engineering problems including failures of quasi-brittle structures and MEMS devices, electrical breakdown of gate dielectrics, and buckling of spherical shells.

The statistical scaling of structural resistance has important consequences for the reliability-based structural design. It has been shown that the safety factors in structural design should vary with the structure size. The size effect on the safety factors is governed by the size effect on the CoV of structural resistance. However, current engineering practice does not account for this size dependence. The consequence of using size-independent safety factors is that structures of different sizes are actually designed against different levels of failure probability, which can potentially exceed the intended tolerable level.

While this paper focuses on the recent developments in probabilistic models for localization-induced failures, there is a considerable interest in developing a general probabilistic model of structural resistance that can be applied to both localized and distributed failures. A notable recent advancement along this line is the fishnet model [95–98], in which the structural failure probability is calculated by explicitly considering the possibility of sequential formation of multiple localized failure zones. The fishnet model was formulated in a discrete framework, which provided a way to bridge the finite weakest-link model and the fiber-bundle model for simple structural geometries. The continuum counterpart of the fishnet model is a level excursion model, which considers sequential crossings. To deal with sequential crossings, one would need to deal with a non-Gaussian, nonstationary random field, a well-known challenge in stochastic mechanics. Mathematical treatment of the sequential level crossing model is a worthwhile subject to investigate in the future, which could lead to a comprehensive mathematical model for probabilistic structural failures.

Funding Data

- Division of Civil, Mechanical, and Manufacturing Innovation, U.S. National Science Foundation to the University of Minnesota (Grant No. Grant CMMI-2151209; Funder ID: 10.13039/100000147).

Data Availability Statement

The datasets generated and supporting the findings of this article are obtainable from the corresponding author upon reasonable request.

References

[1] Bažant, Z. P., 1976, "Instability, Ductility, and Size Effect in Strain-Softening Concrete," J. Eng. Mech. Div. ASCE, **102**(2), pp. 331–344.
[2] Bažant, Z. P., and Planas, J., 1998, *Fracture and Size Effect in Concrete and Other Quasibrittle Materials*, CRC Press, Boca Raton, FL.
[3] Kemeny, J. M., and Cook, N. G. W., 1987, "Crack Models for the Failure of Rock Under Compression," *Proceedings of Second International Conference on Constitutive Laws for Engineering Materials*, C. S. Desai, E. Krempl, P. D. Kiousis, and T. Kundu, eds., Vol. 2, Elsevier, New York, pp. 879–887.
[4] Bésuelle, P., 2001, "Compacting and Dilating Shear Bonds in Porous Rock: Theoretical and Experimental Conditions," J. Geophys. Res., **106**(B7), pp. 13435–13442.
[5] Rudnicki, J. W., 2002, "Conditions for Compaction and Shear Bands in a Transversely Isotropic Material," Int. J. Solids Struct., **39**(13–14), pp. 3741–3756.
[6] Bažant, Z. P., and Kazemi, M. T., 1991, "Size Effect on Diagonal Shear Failure of Beams Without Stirrups," ACI Struct. J., **88**, pp. 268–276.
[7] Syroka-Korol, E., and Tejchman, J., 2014, "Experimental Investigation of Size Effect in Reinforced Concrete Beams Failing by Shear," Eng. Struct., **58**, pp. 63–78.
[8] Yu, Q., Le, J.-L., Hubler, M. H., Wendner, R., Cusatis, G., and Bažant, Z. P., 2016, "Comparison of Main Models for Size Effect on Shear Strength of Reinforced and Prestressed Concrete Beams," Struct. Concrete (Fib), **17**(5), pp. 778–789.
[9] Kármán, T. V., and Tsien, H.-S., 1939, "The Buckling of Spherical Shells by External Pressure," J. Aeronaut. Sci., **7**(2), pp. 43–50.
[10] Horák, J., Lord, G. J., and Peletier, M., 2006, "Cylinder Buckling: The Mountain Pass as an Organizing Center," SIAM J. Appl. Math., **66**(5), pp. 1793–1824.
[11] Kreilos, T., and Schneider, T. M., 2017, "Fully Localized Post-Buckling States of Cylindrical Shells Under Axial Compression," Proc. R. Soc. London A, **473**(2205), p. 20170177.
[12] Audoly, B., and Hutchinson, J. W., 2020, "Localization in Spherical Shell Buckling," J. Mech. Phys. Solids, **136**, p. 103720.
[13] Wilk, G. D., Wallace, R. M., and Anthony, J. M., 2001, "High-k Gate Dielectrics: Current Status and Materials Properties Considerations," J. Appl. Phys., **89**(10), pp. 5243–5275.
[14] Chatterjee, S., Kuo, Y., Lu, J., Tewg, J.-Y., and Majhi, P., 2006, "Electrical Reliability Aspects of HfO_2 High-k Gate Dieletrics With Tan Metal Gate Electrodes Under Constant Voltage Stress," Microelectron. Reliab., **46**(1), pp. 69–76.
[15] Le, J.-L., Bažant, Z. P., and Bazant, M. Z., 2009, "Lifetime of High-k Gate Dielectrics and Analogy With Strength of Quasi-Brittle Structures," J. Appl. Phys., **106**, p. 104119.
[16] Hill, R., 1952, "On Discontinuous Plastic States, With Special Reference to Localized Necking in Thin Sheets," J. Mech. Phys. Solids, **1**(1), pp. 19–30.
[17] Rudnicki, J. W., and Rice, J. R., 1976, "A Conditions for the Localization of Deformation in Pressure-Sensitive Dilatant Materials," J. Mech. Phys. Solids, **23**(6), pp. 371–394.
[18] Rizzi, E., Carol, I., and Willam, K., 1995, "Localization Analysis of Elastic Degradation With Application to Scalar Damage," J. Eng. Mech. ASCE, **121**(4), pp. 541–554.
[19] Jirásek, M., 2007, "Mathematical Analysis of Strain Localization," Rev. Eur. Gén. Civ., **11**(7–8), pp. 977–991.
[20] Bažant, Z. P., and Oh, B.-H., 1983, "Crack Band Theory for Fracture of Concrete," Mater. Struct., **16**, pp. 155–177.
[21] Oliver, J., 1989, "A Consistent Characteristic Length for Smeared Cracking Models," Int. J. Numer. Meth. Eng., **28**, pp. 461–474.
[22] Jirásek, M., and Bauer, M., 2012, "Numerical Aspects of the Crack Band Approach," Comp. Struct., **110-111**, pp. 60–78.
[23] Gorgogianni, A., Eliáš, J., and Le, J.-L., 2020, "Mechanism-Based Energy Regularization in Computational Modeling of Quasibrittle Fracture," ASME J. Appl. Mech., **87**(9), p. 091003.
[24] Pijaudier-Cabot, G., and Bažant, Z. P., 1987, "Nonlocal Damage Theory," J. Eng. Mech. ASCE, **113**(10), pp. 1512–1533.
[25] Bažant, Z. P., and Pijaudier-Cabot, G., 1988, "Nonlocal Continuum Damage, Localization Instability and Convergence," ASME J. Appl. Mech., **55**(2), pp. 287–293.
[26] Bažant, Z. P., and Jirásek, M., 2002, "Nonlocal Integral Formulations of Plasticity and Damage: Survey of Progress," J. Eng. Mech. ASCE, **128**(11), pp. 1119–1149.
[27] Aifantis, E. C., 1984, "On the Microstructural Origin of Certain Inelastic Models," ASME J. Eng. Mater. Technol., **106**(4), pp. 326–330.
[28] Bažant, Z. P., 1984, "Imbricate Continuum and Progressive Fracturing of Concrete and Geomaterials," Meccanica, **19**(S1), pp. 86–93.
[29] Mühlhaus, H.-B., and Alfantis, E. C., 1991, "A Variational Principle for Gradient Plasticity," Int. J. Solids Struct., **28**(7), pp. 845–857.
[30] Peerlings, R. H. J., de Borst, R., Brekelmans, W. A. M., and de Vree, J. H. P., 1996, "Gradient Enhanced Damage for Quasi-Brittle Materials," Int. J. Numer. Methods Eng., **39**(19), pp. 3391–3403.
[31] Peerlings, R. H. J., Geers, M. G. D., de Borst, R., and Brekelmans, W. A. M., 2001, "A Critical Comparison of Nonlocal and Gradient-Enhanced Softening Continua," Int. J. Solids Struct., **38**(44–45), pp. 7723–7746.
[32] Bažant, Z. P., 2004, "Scaling Theory of Quasibrittle Structural Failure," Proc. Natl. Acad. Sci. U. S. A., **101**(37), pp. 13400–13407.
[33] Bažant, Z. P., 2005, *Scaling of Structural Strength*, Elsevier, London, UK.
[34] Bažant, Z. P., and Le, J.-L., 2017, *Probabilistic Mechanics of Quasibrittle Structures: Strength, Lifetime, and Size Effect*, Cambridge University Press, Cambridge, UK.
[35] Bažant, Z. P., Le, J.-L., and Salviato, M., 2021, *Quasibrittle Fracture Mechanics: A First Course*, Oxford University Press, Oxford, UK.
[36] Lee, A., López, J. M., Marthelot, J., Hutchinson, J. W., and Reis, P. M., 2016, "The Geometric Role of Precisely Engineered Imperfections on the Critical Buckling Load of Spherical Elastic Shells," ASME J. Appl. Mech., **83**(11), p. 111005.
[37] Wang, H., Guilleminot, J., Schafer, B. W., and Tootkaboni, M., 2022, "Stochastic Analysis of Geometrically Imperfect Thin Cylindrical Shells Using Topology-Aware Uncertainty Models," Comput. Methods Appl. Mech. Eng., **393**, p. 114780.

[38] Derveni, F., Gueissaz, W., Yan, D., and Reis, P. M., 2023, "Probabilistic Buckling of Imperfect Hemispherical Shells Containing a Distribution of Defects," Philos. Trans. R. Soc. A, **381**(2244), p. 20220298.
[39] Baizhikova, Z., Ballarini, R., and Le, J.-L., 2024, "Uncovering the Dual Role of Dimensionless Radius in Buckling of Spherical Shells With Random Geometric Imperfection," Proc. Natl. Acad. Sci. U. S. A., **121**(16), p. e2322415121.
[40] da Vinci, L., 1881–91, *The Notebook of Leonardo da Vinci* (1945), Edward McCurdy, London, p. 546; *and Les Manuscrits de Léonard de Vinci*, 1500 s, Translated in French by C. Ravaisson-Mollien, Institut de France, London, Vol. 3.
[41] Mariotte, E., 1740, *Traité du mouvement des eaux, posthumously*, edited by M. de la Hire; English Translated by J. T. Desvaguliers, also Marriotte's Collected Works, 2nd ed., The Hague, London (1718), p. 249, p. 1686.
[42] Fisher, R. A., and Tippet, L. H. C., 1928, "Limiting Form of the Frequency Distribution the Largest and Smallest Number of a Sample," Proc. Cambridge Philos. Soc., **24**(2), pp. 180–190.
[43] Weibull, W., 1939, "The Phenomenon of Rupture in Solids," Proc. R. Sweden Inst. Eng. Res., **153**, pp. 1–55.
[44] Weibull, W., 1951, "A Statistical Distribution Function of Wide Applicability," ASME J. Appl. Mech., **18**(3), pp. 293–297.
[45] Bažant, Z. P., and Pang, S. D., 2006, "Mechanics Based Statistics of Failure Risk of Quasibrittle Structures and Size Effect on Safety Factors," Proc. Natl. Acad. Sci. U. S. A., **103**(25), pp. 9434–9439.
[46] Bažant, Z. P., and Pang, S. D., 2007, "Activation Energy Based Extreme Value Statistics and Size Effect in Brittle and Quasibrittle Fracture," J. Mech. Phys. Solids, **55**(1), pp. 91–131.
[47] Bažant, Z. P., Le, J.-L., and Bazant, M. Z., 2009, "Scaling of Strength and Lifetime Distributions of Quasibrittle Structures Based on Atomistic Fracture Mechanics," Proc. Natl. Acad. Sci. U. S. A., **106**, pp. 11484–11489.
[48] Le, J.-L., Bažant, Z. P., and Bazant, M. Z., 2011, "Unified Nano-Mechanics Based Probabilistic Theory of Quasibrittle and Brittle Structures: I. Strength, Crack Growth, Lifetime and Scaling," J. Mech. Phys. Solids, **59**, pp. 1291–1321.
[49] Xu, Z., and Le, J.-L., 2017, "A First Passage Model for Probabilistic Failure of Polycrystalline Silicon MEMS Structures," J. Mech. Phys. Solids, **99**, pp. 225–241.
[50] Xu, Z., and Le, J.-L., 2018, "On Power-Law Tail Distribution of Strength Statistics of Brittle and Quasibrittle Structures," Eng. Frac. Mech., **197**, pp. 80–91.
[51] Le, J.-L., 2020, "Level Excursion Analysis of Probabilistic Quasibrittle Fracture," Sci. China Tech. Sci., **63**, pp. 1141–1153.
[52] Gumbel, E. J., 1958, *Statistics of Extremes*, Columbia University Press, New York.
[53] Ang, A. H. S., and Tang, W. H., 1984, *Probability Concepts in Engineering Planning and Design*, Vol. II (*Decision, Risk and Reliability*), John Wiley, New York.
[54] Vanmarcke, E., 2010, *Random Fields Analysis and Synthesis*, World Scientific Publishers, Singapore.
[55] Gnedenko, B. V., 1943, "Sur la Distribution Limite du Terme Maximum D'une Serie Aleatoire," Ann. Math., **44**, pp. 423–453.
[56] Castillo, E., 1988, *Extreme Value Theory in Engineering*, Academic Press, San Diego, CA.
[57] Barenblatt, G. I., 1996, *Scaling, Self-Similarity, and Intermediate Asymptotics*, Cambridge University Press, Cambridge, UK.
[58] Barenblatt, G. I., 2003, *Scaling*, Cambridge University Press, Cambridge, UK.
[59] Le, J.-L., Cannone Falchetto, A., and Marasteanu, M. O., 2013, "Determination of Strength Distribution of Quasibrittle Structures From Mean Size Effect Analysis," Mech. Mater., **66**, pp. 79–87.
[60] Le, J.-L., 2015, "Size Effect on Reliability Indices and Safety Factors of Quasibrittle Structures," Struct. Saf., **52**, pp. 20–28.
[61] Vanmarcke, E. H., 1975, "On the Distribution of the First-Passage Time for Normal Stationary Random Processes," ASME J. Appl. Mech., **42**(1), pp. 215–220.
[62] Vořechovský, M., and Eliáš, J., 2020, "Fracture in Random Quasibrittle Media: II. Analytical Model Based on Extremes of the Averaging Process," Eng. Frac. Mech., **235**, p. 107155.
[63] Grigoriu, M., 1984, "Crossings of non-Gaussian Translation Processes," J. Eng. Mech. ASCE, **110**(4), pp. 610–620.
[64] Grigoriu, M., 1998, "Simulation of Stationary Non-Gaussian Translation Processes," J. Eng. Mech. ASCE, **124**(2), pp. 121–126.
[65] Adler, R. J., 2000, "On Excursion Sets, Tube Formulas and Maxima of Random Fields," Ann. Appl. Prob., **10**(1), pp. 1–74.
[66] Adler, R. J., and Taylor, J. E., 2009, *Random Fields and Geometry*, Springer Science & Business Media, New York.
[67] Abramowitz, M., and Stegun, I. A., 1964, *Handbook of Mathematical Functions: With Formulas, Graphs, and Mathematical Tables*, Vol. 55, Courier Corporation, New York.
[68] Ripley, B. D., 2005, *Spatial Statistics*, Vol. 575, Wiley, Hoboken, NJ.
[69] Abrahamsen, P., 1997, *A Review of Gaussian Random Fields and Correlation Functions*, Norsk Regnesentral/Norwegian Computing Center, Oslo, Norway.
[70] Fontana, J., and Palffy-Muhoray, P., 2020, "St. Petersburg Paradox and Failure Probability," Phys. Rev. Lett., **124**, p. 245501.
[71] Eliáš, J., and Le, J.-L., 2024, "Size Effect on Strength Statistics of Prenotched Quasibrittle Structures," J. Eng. Mech. ASCE, **150**(6), p. 04024025.
[72] Salem, J. A., Nemeth, N. N., Powers, L. P., and Choi, S. R., 1996, "Reliability Analysis of Uniaxially Ground Brittle Materials," ASME Eng. Gas Turbines Power, **118**(4), pp. 863–871.
[73] Gross, B., 1996, "Least Squares Best Fit Method for the Three Parameter Weibull Distribution: Analysis of Tensile and Bend Specimens With Volume or Surface Flaw Failure," NASA, Cleveland, OH, Report No. TM-4721, pp. 1–21.
[74] Santos, C. D., Strecker, K., Piorino Neto, F., Silva, O. M. D. M., Baldacim, S. A., and Silva, C. R. M. D., 2003, "Evaluation of the Reliability of Si_3N_4-Al_2O_3 -CTR_2O_3 Ceramics Through Weibull Analysis," Mater. Res., **6**(4), pp. 463–467.
[75] Hazra, S. S., Baker, M. S., Beuth, J. L., and de Boer, M. P., 2009, "Demonstration of an In-Situ On-Chip Tester," J. Micromech. Microeng., **19**(8), p. 082001.
[76] Reedy, E. D., Boyce, B. L., Foulk, J. W., Field, R. V., de Boer, M. P., and Hazra, S. S., 2011, "Predicting Fracture in Micrometer-Scale Polycrystalline Silicon MEMS Structures," J. Microelectromech. Syst., **20**(4), pp. 922–932.
[77] Rice, S. O., 1944, "Mathematical Analysis of Random Noise," Bell Labs Tech. J., **23**(3), pp. 282–332.
[78] Saleh, M. E., Beuth, J. L., and de Boer, M. P., 2014, "Validated Prediction of the Strength Size Effect in Polycrystalline Silicon Using the Three-Parameter Weibull Function," J. Amer. Cer. Soc., **97**(12), pp. 3982–3990.
[79] Le, J.-L., and Eliáš, J., 2016, "A Probabilistic Crack Band Model for Quasibrittle Fracture," ASME J. Appl. Mech., **83**(5), p. 051005.
[80] Gorgogianni, A., Elias, J., and Le, J.-L., 2022, "Mesh Objective Stochastic Simulations of Quasibrittle Fracture," J. Mech. Phys. Solids, **159**, p. 104745.
[81] Vievering, J., and Le, J.-L., 2024, "Mechanism-Based Mapping of Random Fields for Stochastic FE Simulations of Quasibrittle Fracture," J. Mech. Phys. Solids, **186**, p. 105578.
[82] Bažant, Z. P., and Cedolin, L., 1991, *Stability of Structures: Elastic, Inelastic, Fracture and Damage Theories*, Oxford University Press, New York.
[83] Koiter, W. T., 1945, *Over de stabiliteit van het elastisch evenwicht*, Ph.D. thesis, Delft University of Technology, Amsterdam, The Netherlands.
[84] Hutchinson, J. W., and Koiter, W. T., 1970, "Postbuckling Theory," Appl. Mech. Rev. ASME, **23**(12), pp. 1353–1366.
[85] Bolotin, V. V., 1962, "Statistical Methods in the Nonlinear Theory of Elastic Shells," NASA, Washington, DC, Report No. TT F-85.
[86] Amazigo, J. C., 1969, "Buckling Under Axial Compression of Long Cylindrical Shells With Random Axisymmetric Imperfections," Quart. Appl. Math., **26**(4), pp. 537–566.
[87] Elishakoff, I., and Cai, G. Q., 1994, "Nonlinear Buckling of a Column With Initial Imperfection Via Stochastic and Non-Stochastic Convex Models," Int. J. Non-Linear Mech., **29**, pp. 71–82.
[88] Elishakoff, I., 2000, "Uncertain Buckling: Its Past, Present and Future," Int. J. Solids Struct., **37**(46–47), pp. 6869–6889.
[89] Tsien, H.-S., 1942, "A Theory for the Buckling of Thin Shells," J. Aeronaut. Sci., **9**(10), pp. 373–384.
[90] Le, J.-L., 2012, "A Finite Weakest Link Model of Lifetime Distribution of High-Kgate Dielectrics Under Unipolar AC Voltage Stress," Microelectron. Reliab., **52**(1), pp. 100–106.
[91] American Concrete Institute, 2019, *Building Code Requirements for Structural Concrete*, American Concrete Institute, Farmington Hills, MI, Report No. ACI 318–19.
[92] Nozawa, T., Kim, S., Ozawa, K., and Tanigawa, H., 2014, "Stress Envelope of Silicon Carbide Composites at Elevated Temperatures," Fusion Eng. Des., **89**(7), pp. 1723–1727.
[93] Cornell, C. A., 1969, "A Probability-Based Structural Code," J. Amer. Concr. Inst., **66**(12), pp. 974–985.
[94] Haldar, A., and Mahadevan, S., 2000, *Probability, Reliability, and Statistical Methods in Engineering Design*, Wiley, New York.
[95] Luo, W., and Bažant, Z. P., 2017, "Fishnet Model for Failure Probability Tail of Nacre-Like Imbricated Lamellar Materials," Proc. Natl. Acad. Sci. U. S. A., **114**(49), pp. 12900–12905.
[96] Luo, W., and Bažant, Z. P., 2017, "Fishnet Statistics for Probabilistic Strength and Scaling of Nacreous Imbricated Lamellar Materials," J. Mech. Phys. Solids, **109**, pp. 264–287.
[97] Luo, W., and Bažant, Z. P., 2018, "Fishnet Model With Order Statistics for Tail Probability of Failure of Nacreous Biomimetic Materials With Softening Interlaminar Links," J. Mech. Phys. Solids, **121**, pp. 281–295.
[98] Xu, H., Vievering, J., Nguyen, H. T., Zhang, Y., Le, J.-L., and Bažant, Z. P., 2024, "Asymptotically Matched Extrapolation of Fishnet Failure Probability to Continuum Scale," J. Mech. Phys. Solids, **182**, p. 105479.